NAVAL POSTGRADUATE SCHOOL

MONTEREY, CALIFORNIA

THESIS

EXPERIMENTAL STUDY OF SOLDER/COPPER INTERFACE FAILURE UNDER VARYING STRAIN RATES

by

Andrew Michael Luteran

March 2011

Thesis Advisor:	Young W. Kwon
Second Reader:	Jarema M. Didoszak

Approved for public release; distribution is unlimited

THIS PAGE INTENTIONALLY LEFT BLANK

REPORT DOCUMENTATION PAGE			Form Approved OMB No. 0704-0188
Public reporting burden for this collection of information is estimated to average 1 hour per response, including the time for reviewing instruction, searching existing data sources, gathering and maintaining the data needed, and completing and reviewing the collection of information. Send comments regarding this burden estimate or any other aspect of this collection of information, including suggestions for reducing this burden, to Washington headquarters Services, Directorate for Information Operations and Reports, 1215 Jefferson Davis Highway, Suite 1204, Arlington, VA 22202-4302, and to the Office of Management and Budget, Paperwork Reduction Project (0704-0188) Washington DC 20503.			
1. AGENCY USE ONLY ***(Leave blank)***	**2. REPORT DATE** March 2011	**3. REPORT TYPE AND DATES COVERED** Master's Thesis	
4. TITLE AND SUBTITLE Experimental Study of Solder/Copper Interface Failure Under Varying Strain Rates			**5. FUNDING NUMBERS**
6. AUTHOR(S) Andrew Michael Luteran			
7. PERFORMING ORGANIZATION NAME(S) AND ADDRESS(ES) Naval Postgraduate School Monterey, CA 93943-5000			**8. PERFORMING ORGANIZATION REPORT NUMBER**
9. SPONSORING /MONITORING AGENCY NAME(S) AND ADDRESS(ES) N/A			**10. SPONSORING/MONITORING AGENCY REPORT NUMBER**
11. SUPPLEMENTARY NOTES The views expressed in this thesis are those of the author and do not reflect the official policy or position of the Department of Defense or the U.S. Government.			
12a. DISTRIBUTION / AVAILABILITY STATEMENT Approved for public release; distribution unlimited			**12b. DISTRIBUTION CODE**

13. ABSTRACT

This thesis investigates the mechanical behavior of the copper-solder interface when subjected to dynamic axial loads at strain rates between 10.0 s^{-1} and 0.05 s^{-1}. The copper is alloy 101 and the lead-free solder has a composition of 96% tin and 4% silver. The tests results revealed that as the strain rate increases so do the ultimate and yield strengths but the elastic modulus diminishes. When the specimens were heated to 65.5 degrees Celsius, the ultimate and yield strengths were significantly lower. Specimens were also tested at varying strain rates to compare and contrast the differences with the single strain rate data. Analysis of the fracture strain of the single and multiple strain rate tests revealed that the fracture strain from multiple-strain rate loadings fell between the fracture strains of the two single-strain rates. From this observation, simple averaging could be utilized to predict the fracture strain when a copper-solder specimen was subjected to varying strain rates.

14. SUBJECT TERMS dynamic axial loads, lead-free solder, solder joints, varying strain rate, copper-solder interface			**15. NUMBER OF PAGES** 79
			16. PRICE CODE
17. SECURITY CLASSIFICATION OF REPORT Unclassified	**18. SECURITY CLASSIFICATION OF THIS PAGE** Unclassified	**19. SECURITY CLASSIFICATION OF ABSTRACT** Unclassified	**20. LIMITATION OF ABSTRACT** UU

NSN 7540-01-280-5500 Standard Form 298 (Rev. 2-89)
Prescribed by ANSI Std. 239-18

THIS PAGE INTENTIONALLY LEFT BLANK

Approved for public release; distribution is unlimited

EXPERIMENTAL STUDY OF SOLDER/COPPER INTERFACE UNDER VARYING STRAIN RATES

Andrew M. Luteran
Lieutenant, United States Navy
B.S., Wichita State University, 2004

Submitted in partial fulfillment of the
requirements for the degree of

MECHANICAL ENGINEER
AND
MASTER OF SCIENCE IN MECHANICAL ENGINEERING

from the

NAVAL POSTGRADUATE SCHOOL
March 2011

Author: Andrew M. Luteran

Approved by: Young W. Kwon
Thesis Advisor

Jarema M. Didoszak
Second Reader

Knox T. Millsaps
Chairman, Department of Mechanical and Aerospace Engineering

THIS PAGE INTENTIONALLY LEFT BLANK

ABSTRACT

This thesis investigates the mechanical behavior of the copper-solder interface when subjected to dynamic axial loads at strain rates between 10.0 s^{-1} and 0.05 s^{-1}. The copper is alloy 101 and the lead-free solder has a composition of 96% tin and 4% silver. The tests results revealed that as the strain rate increases so do the ultimate and yield strengths but the elastic modulus diminishes. When the specimens were heated to 65.5 degrees Celsius, the ultimate and yield strengths were significantly lower. Specimens were also tested at varying strain rates to compare and contrast the differences with the single strain rate data. Analysis of the fracture strain of the single and multiple strain rate tests revealed that the fracture strain from multiple-strain rate loadings fell between the fracture strains of the two single-strain rates. From this observation, simple averaging could be utilized to predict the fracture strain when a copper-solder specimen was subjected to varying strain rates.

THIS PAGE INTENTIONALLY LEFT BLANK

TABLE OF CONTENTS

THIS PAGE INTENTIONALLY LEFT BLANK

LIST OF FIGURES

THIS PAGE INTENTIONALLY LEFT BLANK

LIST OF TABLES

THIS PAGE INTENTIONALLY LEFT BLANK

LIST OF ACRONYMS AND ABBREVIATIONS

Ag	Element symbol for silver
COTS	Commercial-off-the-shelf
Cu	Element symbol for Copper
ε	Strain (mm/mm)
$\dot{\varepsilon}$	Strain rate (s^{-1})
FE	Finite Element
in	Inches
JEDEC	Joint Electron Devices Engineering Council
k	Kilo
l	Length
M	Mega
mm	millimeters
PCB	Printed Circuit Board
SEM	Scanning Electron Microscope
s	Seconds
Sn	Element symbol for Tin
V	Velocity

THIS PAGE INTENTIONALLY LEFT BLANK

ACKNOWLEDGMENTS

I would like to thank Professor Young Kwon for his guidance and patience throughout the course of this thesis work. I would also like to thank Professor Jarema Didoszak for his insight in completing this research. Finally, I would like to thank my wife, Mary, for all her love and support.

THIS PAGE INTENTIONALLY LEFT BLANK

I. INTRODUCTION

The vast majority of failures in electronic equipment are due to failures in the solder joint that connects the electronic component to the printed circuit board. The failure at the solder joint can be from a number of circumstances from poor quality control in the manufacturing process, changes in the operating environment such as temperature and humidity, and vibration and shock.

Twenty percent of solder joint failures are due to vibration and shock. Electronic equipment used in a military environment will undergo significant levels of shock and vibration loading that well exceeds that typically found in commercial applications [1]. A naval vessel that experiences an underwater explosion, for instance, would be subject to a large initial shock and followed by subsequent shocks of less magnitude. This would be analogous to a solder joint that is subject to a high strain rate loading followed by lower strain rate loads. As the strain rate varies, the strength of the solder joint may also vary. The differences of strength may differ significantly from static loading conditions. Therefore, continued research on the effect of varying strain rates on the strength of the solder joint is beneficial to the design of electronic equipment and the formulation of a criterion for predicting failure of solder joints.

A. LITERATURE REVIEW

The literature review shows research previously completed related to solder joint failure. This will include the effects of vibration on the joints as well as the effects of strain rate variation.

1. Factors Affecting Solder Joint Reliability

Gu *et al.* [1] determined that during the life cycle of electronic assemblies, approximately 55 percent of failures are due to extreme temperatures and temperature cycling, which cause thermal stresses in the electronic assemblies. Twenty percent are related to vibration and shock, with the remaining percentage associated with changes in

humidity. Research conducted by Ross *et al.* [2] adds that creep strain is the most important time-dependent factor affecting the reliability of solder joints in electronic equipment.

2. Effects of Vibration on Solder Joints

Celik and Genc [3] investigated the vibration induced fatigue life analysis on an axial leaded aluminum capacitor. The choice of the component is unique as it is not surface mount technology, but considered as "through-hole" technology. This component is subject to failures in the solder joint, lead wires, and internal components. The component is most likely to fail due to flexure of the printed circuit board (PCB) to which it is soldered.

Celik and Genc stated that many military systems use commercial-off-the-shelf (COTS) products in the development of the electronic systems. The COTS electronics have an expected life expectancy of 7–10 years whereas electronics designed specifically for military use have a life expectancy of up to 20 years.

Celik and Genc focused their research on stress-induced failures due to vibrations. They performed a method of testing known as step stress testing. This testing approach determines the design limit of the printed circuit boards. This method subjects a printed circuit board to a series of high steps of stress. The advantage of this testing method takes the printed circuit board to the level of failure in a relatively short length of time.

Celik and Genc conducted two tests and numerous failures were detected in both tests. All the failures were due to stress from the flexing of the printed circuit board. Flexure stress on the leads was most significant during the first test while the second test produced solder joint failure.

The conclusion that Celik and Genc arrived at was that industry should use more simulations to predict the failure of components. They realized that field-testing to improve systems is not always practical. In addition, the use of isolators to protect COTS electronics is not always practical in military hardware applications due to their size and costs.

3. Effects of Strain Rate Variations on Solder Joints

Su *et al*. [4], and Pang and Che [5] have determined with portable consumer electronic devices growing ever smaller, the solder joints which are associated with the components inside the devices also are growing smaller. This miniaturization of electronics presents a mechanical challenge for solder joint reliability especially at high strain rates. The electronic devices will come under high strain rates during testing, shipping and under field use by the end consumer.

Su *et al.* performed pull and shear tests on wafer level chip scale packages using different lead-free solder at strain rates of 2.27 s^{-1} and 22.73 s^{-1}. They observed that more interface failures occurred at higher strain rates, whereas at lower strain rates, failure occurred in the bulk of the solder. The content of silver (Ag) present in the solder produced different results on the type of failure that occurred. The higher the Ag content generally yielded more interface failures and lower peak loads.

Su *et al.* concluded that having more bulk solder failures and a higher solder joint array strength are desired characteristics to have better mechanical reliability of solder joints in the electronic equipment.

Similar results occurred during research of this thesis. These results are outlined in the Chapter III under the Scanning Electron Microscope.

4. Solder Joint Reliability Prediction, Assessment and Recording Methods

Bayes [6] concluded that in an ideal world each individual product would be tested at its final stage to determine its capability. He realized that in the real-world environment this was not practical and that extrapolations from a number of tests that are not product specific would have to be made. Bayes recommended testing the product and its components at different stages of production. The different level of stages recommended is the materials level, assembly level, test panel level and the product level. The materials level would test the quality of the material, such as solderability, the assembly level would test continuity between components which could indicate faulty solder joints, the test panel level would be a test of an assembly with power supplied to

ensure connectivity between the components and lastly, testing at the product level. The product level testing would mimic usage of the product by the end-use to ensure functionality of the product under normal conditions. This level of testing would not check for solder joint reliability by vibration and shock but more the reliability of the joints from thermal stresses and power on/off cycling.

JEDEC [7], formally known as the Joint Electron Devices Engineering Council, has formulated a standard for the shock testing of electronic devices in order to test solder joint reliability. The intention of JEDEC is to improve upon past mechanical shock test methods and tie the test conditions back to the conditions the electronic device would experience by the end-user.

A complete description of JEDEC mechanical testing and drop impact methods can be found in [7], but Qin *et al.* [8] gives an excellent description of a drop impact test and it is provided here as an example. The JEDEC impact test setup is similar to that in Figure 1. The impact test consists of a PCB and an electronic component that is bolted onto a metal plate. The entire assembly is subject to a free fall along guideposts from a predetermined height. At the conclusion of the free fall, the metal base impacts a rigid foundation, which then creates an impact loading on the assembly. A half-sine acceleration pulse can be achieved by adjusting the drop height and the size and consistency of the cushion pads. The stiffness of the metal plate is much greater than that of the PCB resulting in the half-sine acceleration pulse from the impact to be transmitted with little distortion via the mounting bolts to the PCB. Therefore, the board level drop impact test can be modeled as if the PCB was subjected a half-sine acceleration via the mounting bolts.

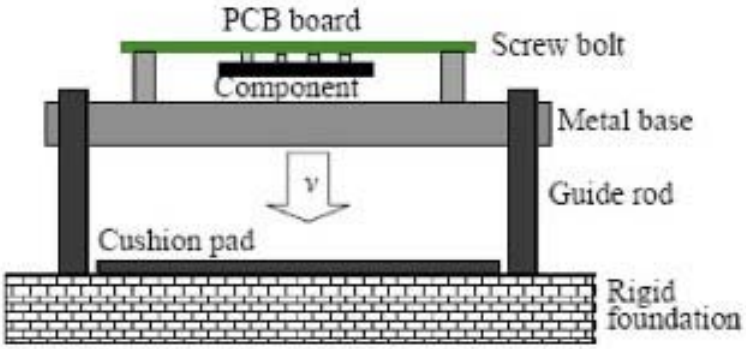

Figure 1. Example of a JEDEC test set-up From [8].

JEDEC collects test data and makes recommendations based on the results. JEDEC in no way recommends on how electronic equipment should be engineered but what rather on what use conditions will cause solder joint failure.

B. OVERVIEW OF SOLDERING BASICS

The overview of soldering basics will discuss the basics involved in joining two base metals to make a permanent electrical or mechanical connection by the method of soldering. For a complete understanding of the solder joint, an overview of soldering basics is necessary. To complete a joined section, four elements are required: solder, base metal, flux, and heat. Once the solder connection is made, the solder and base form a new alloy different from those of the base metal and solder.

1. Base Metals

The base metal is what the solder comes into contact with during the solder process to form the intermediate alloy. During the manufacturing process, electronic components contain leads that are soldered to the printed circuit board. The most common base metal is copper, but bronze, brass and silver are other metals with good solder properties. Samples of a few metals that do not have good soldering properties are aluminum, cast iron, and titanium. These metals are often used to create the machinery required for the soldering process.

2. Flux

Flux comes in the form of a liquid or a paste and is used in the soldering process to prevent the base metal from oxidizing. The base metal oxidizes when heat is applied and this layer of oxidation directly affects the strength of the solder connection.

When solder is applied to a heated base metal, flux must readily move out of the way of the solder so that the solder can come into contact with the base metal. Therefore, it must melt at a temperature lower than the solder so that the flux can perform its intended function [9]. Inevitably, the flux and solder combine but flux designers take this into account and design flux resins to lower the surface tension of the solder upon contact with the base metal. This flux design allows for more efficient wetting of solder into the base metal [10].

3. Solder

There are many different type of solder in use today. In past years, tin-lead solder was the most popular solder for electronic applications. In recent years, lead-free solder has replaced the lead-tin solder, mainly due to the toxic properties of lead. As electronic components are discarded and find their way to landfills, the lead inevitably finds its way to the water table and into the drinking water supply. The solder used in this research consists of 96% Sn and 4% Ag. Lead-free solder is more expensive than tin-lead solder by a little over 2.5 times [11]. In addition to being more expensive, tin-lead solder also has a melting point that is lower than lead-free solder. The lesser heat is applied to the base metal, the lesser the impact of oxidation is from the heating of the base metal.

4. Methods of Heat Application for Soldering

Three methods of soldering are currently in use in manufacturing or repair of solder joints. The first method to discuss is single point soldering. Single point soldering is the use a soldering iron where the technician has the ability to adjust the temperature of the iron. Second method of soldering is hot air soldering. Hot air soldering is used most commonly for surface mount components, as the leads of the components are either too small or unreachable by a soldering iron. Technicians removing or installing soldered

electronics components on a printed circuit board will most commonly use one of the two aforementioned methods of soldering. The ability of the technician to adjust the temperature of a soldering iron or a hot air soldering machine is important as to reduce the amount of oxidation formed on the base metal. The temperature ideally should be set slightly above the melting temperature of the solder in use.

The third method of soldering is known as wave soldering. This method is most commonly found in manufacturing where printed circuit boards are mass produced and often contain numerous electronic components [12]. This is an automated process where the solder is maintained at the proper temperature.

C. THE WETTING ACTION

Molten solder penetrates the base metal, usually copper in electronic applications, to form a new alloy. The action of the solder penetrating the base metal is what is referred to as “wets the metal” or “the metal is wetted” [13]. The wetting action forms an intermolecular bond between the solder and the base metal. If the base metal contains contaminates or has developed an oxide film, the wetting action will not occur or the quality of the wetting action will be poor as shown in Figure 2. Proper preparation of the surface to be soldered, as well as the use of a flux are essential. In addition, the base metal and solder must reach the proper temperature. The strength of the solder joint between the soldered components is dependent on the proper development of the intermolecular bond. Figure 3 shows a drop of solder on a substrate with flux pre-applied and the wetting action is very good. The angle, phi, can be used to indicate the wettability and different ranges of the angle phi are given in Table 1.

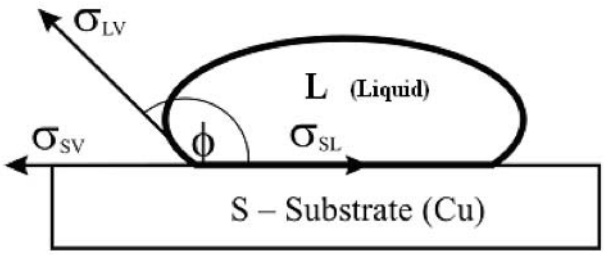

Figure 2. Illustration of Poor Wetting Action From [14].

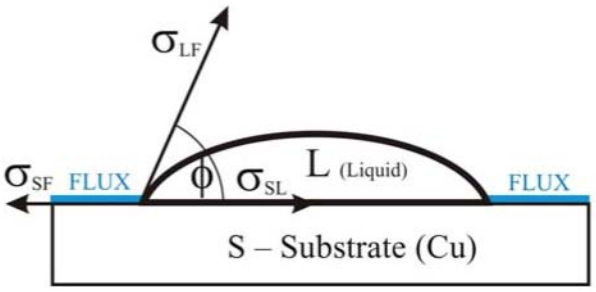

Figure 3. Illustration of Good Wetting Action From [14].

Table 1. Wettability phi angles From [14].

ϕ angle	wettability
0 - 30	very good wetting
30 - 40	good wetting
40 - 55	acceptable
55 - 70	poor wetting
> 70	very poor wetting

D. FORMATION OF A INTER-METALLIC COMPOUND

Solder joints formed using copper as the base material form two compounds between the bulk solder and copper known as Cu_6Sn_5 and Cu_3Sn with the latter forming nearest the copper as illustrated in Figure 4. The thickness and composition of the inter-metallic compounds is a function of three factors: the cleanliness of the copper substrate, the solder chosen, and the assembly process [14].

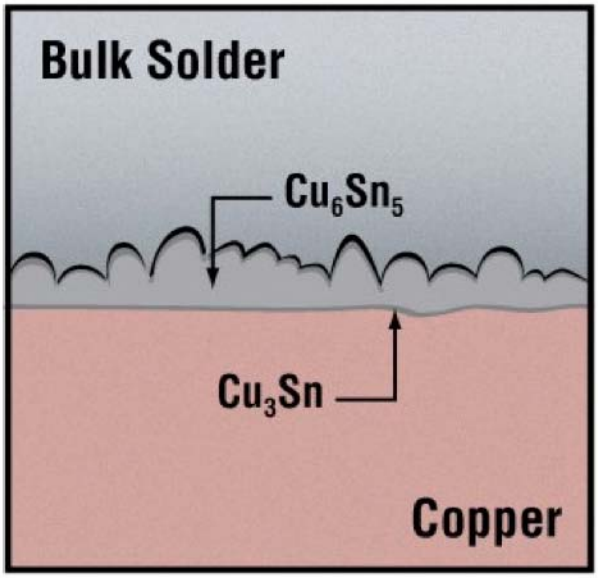

Figure 4. Schematic of the Inter-Metallic Compounds From [6].

The duration and intensity of the heat applied during the soldering process will directly influence the shape and size of the crystalline grains of the intermolecular bond of copper and tin. To achieve a strong bond and an excellent solder joint, fine crystalline structures are desired. This is accomplished by exposing the materials to be soldered to the applied heat for the least amount of time. Longer exposure will result in a coarse crystalline structure and having less shear strength because of being more brittle [13].

E. OBJECTIVES

An objective of this thesis is to examine the mechanical behavior of a solder joint when subjected to dynamic uniaxial loads. In addition, the mechanical behaviors of the solder joint will be examined at room temperature and at an elevated temperature to compare and contrast the difference of the mechanical behavior.

Once the data from the tensile testing is collected and the mechanical behavior of the solder joint are evident, this study will attempt to establish a failure criterion based on dynamic loading when the solder joint is dynamically loaded to strain rates between 0.05 s^{-1} and 10.0 s^{-1}.

Chapter II of this thesis describes the experimental setup and procedures used. Chapter III discusses the results and Chapter IV contains conclusion and recommendations.

II. EXPERIMENTAL SETUP AND PROCEDURES

The material used in the specimens is copper alloy 101 that was soldered together with a lead free solder consisting of 96% tin and 4% silver. The properties of the solder and copper are outlined in Table 2. The flux used was a water-soluble flux in the form of a paste. The copper alloy rods have a diameter of 6.35 mm (0.25 in.) and the end of each copper specimen was cut to a 45-degree angle. The dimensions of the specimens are given in Figure 5.

Table 2. Material Properties.

Properties	**Copper**	**Solder**
Density (g/m^3)	8.9	7.3
Modulus of Elasticity (GPa)	117	56
Melting Point (C)	1082	221
Tensile Strength (MPa)	287	61

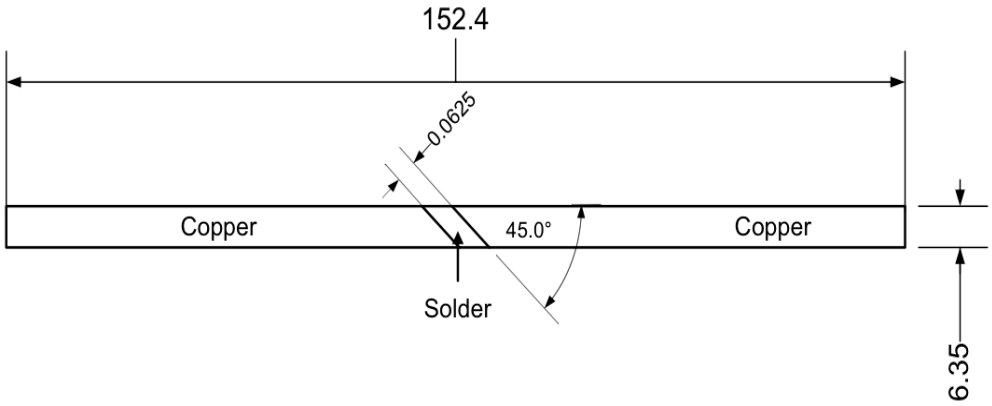

Figure 5. Dimensions of the test specimens in millimeters.

Each specimen was prepared and soldered the same way to ensure consistency during testing. The ends to be soldered were sanded with 640-grit sandpaper to remove

the grooves and swirls that were produced by the machining of the pieces. After sanding, the pieces were cleaned with acetone to remove any impurities and oxidation that may have been present before the application of the flux. The flux paste was applied to each end to be soldered to ensure a proper wetting of the solder to the copper.

An aluminum cast, as shown in Figure 6, was used to hold and protect the copper pieces during the soldering process. Setscrews on the cast allowed the pieces to be held in place once the gap between the pieces was set and the cast itself protected the area to be soldered from the propane flame. The gap between the pieces was set at 1.58 mm (0.125 in.). The protection from the heat source provided by the cast is essential to preventing oxygen from the atmosphere being forced into the molten solder. The introduction of the atmospheric impurities could weaken the solder joint.

Once the pieces were secured with the solder gap set, the aluminum cast was placed in a tabletop vice and a propane torch then applied the heat to the bottom of the aluminum cast. The propane flame remained on the cast until the solder flowed freely into the copper.

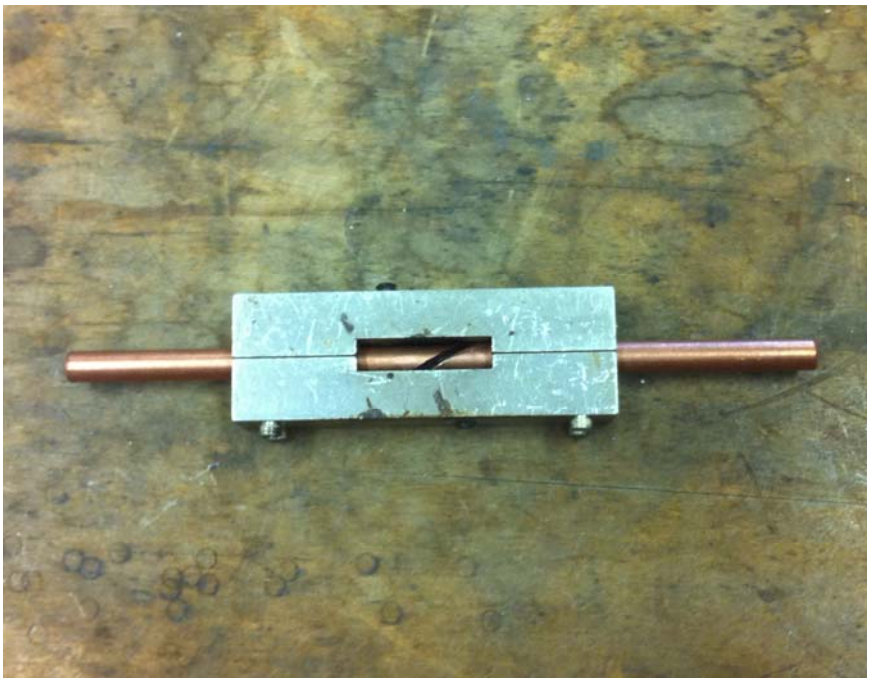

Figure 6. Aluminum cast with copper pieces.

Once the two copper pieces were soldered together, the aluminum cast was allowed to cool to approximately 50.0 degrees Celsius, as measured with an Omega thermometer, model HH21, with a K-type temperature probe. The temperature was taken at the junction of the extruding copper piece and the aluminum cast. Once cooled, the specimen was removed from the cast and allowed to cool to room temperature that averaged 72 degree Fahrenheit. The copper-solder specimen was allowed to set for a minimum of 24 hours prior to tensile testing.

The tensile testing of the specimens was performed using a hydraulic uniaxial tension machine by the MTS Systems Corporation at room temperature. The test data was collected by TestStar IIs Station Manager software, version 3.3B 1205 by the MTS Systems Corporation. The uniaxial tensile testing was performed at the following strain rates from start to specimen fracture: 10.0 s^{-1}, 5.0 s^{-1}, 1.0 s^{-1}, 0.1 s^{-1}, and 0.05 s^{-1}. Strain rate was calculated with Equation (1).

$$\dot{\varepsilon} = \frac{V}{l_o} \tag{1}$$

V and l_0 represent the speed of the testing machine actuator and the gauge length of the specimen respectively. The gauge length of the specimen is the length of the gap between the two copper specimens that is filled with solder. Since the gauge length of the solder stays constant at 1.59 mm, the actuator speed of 15.88 mm/s, 7.94 mm/s, 1.59 mm/s, 0.159 mm/s and 0.079 mm/s were used to achieve the aforementioned strain rates.

Each strain rate was tested at room temperature and the strain rates of 10.0 s^{-1}, 1.0 s^{-1}, and 0.05 s^{-1} were tested at 65.5 degree Celsius (150 degrees Fahrenheit).

Each strain rate test was repeated multiple times to verify the data were consistent and an average was computed. Figure 7 shows a typical stress-strain curve from the copper-solder specimens and allowed the mechanical properties of the specimens to be readily identified and recorded.

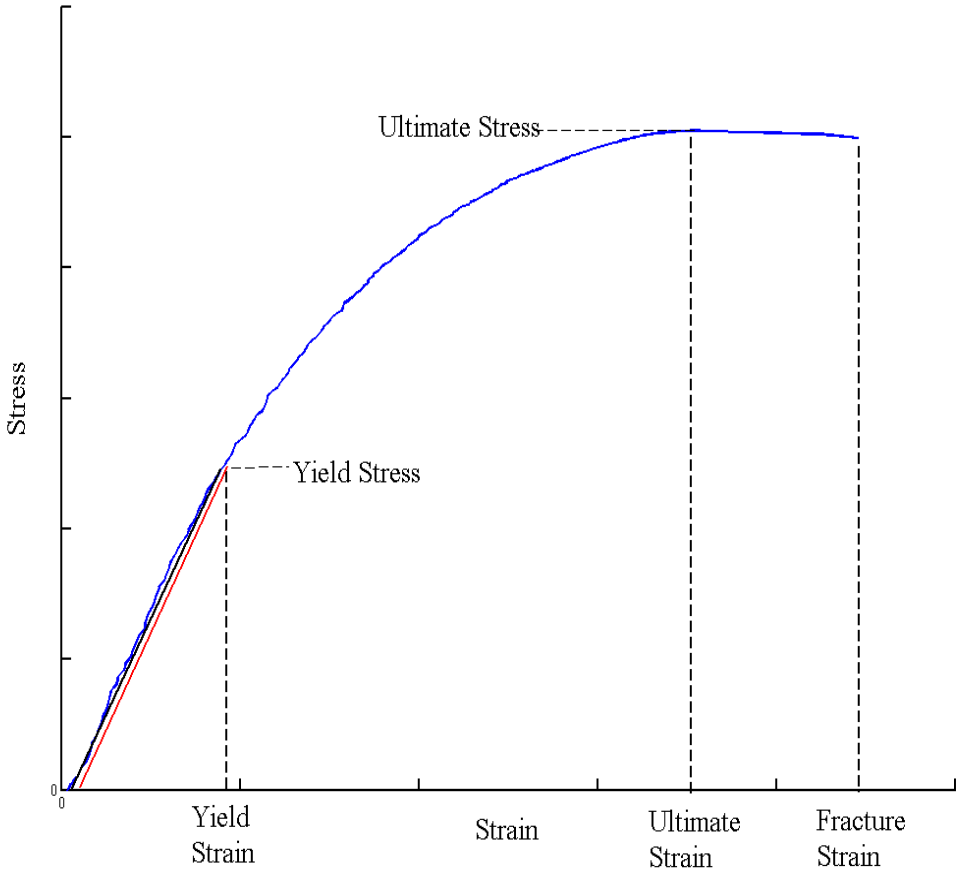

Figure 7. Typical Stress-Strain Curve.

A second set of tests was performed, on the copper-solder specimens, that involved multiple-strain rates. The second set of tests started with an initial strain rate until a predetermined displacement was reached, either before or after yield strength, and then the strain rate would undergo a step change in the strain rate until failure. The specimens were subject to strain rates that varied from fast to slow and slow to fast. Table 3 shows the different strain rates and the strain at which the transition took place between the two strain rates. In addition, the tests performed in Table 3 were repeated at a temperature of 65.5 degrees Celsius.

Table 3. Parameters in varying strain rate tests.

No.	First Strain Rate (1/s)	Second Strain Rate (1/s)	Transition Strain
1*	1.00	0.05	0.016
2*	1.00	0.05	0.020
3*	1.00	0.05	0.027
4^	1.00	0.05	0.047
5^	1.00	0.05	0.0567
6^	1.00	0.05	0.072
7*	0.05	1.00	0.010
8*	0.05	1.00	0.016
9*	0.05	1.00	0.024
10^	0.05	1.00	0.031
11^	0.05	1.00	0.042
12^	0.05	1.00	0.057

*: denotes transition strain is before yield strength

^: denotes transition strain is after yield strength

The purpose of varying the strain rates is to examine the criterion for the copper-solder interface failure under dynamic loading.

THIS PAGE INTENTIONALLY LEFT BLANK

III. RESULTS AND DISCUSSION

A. SCANNING ELECTRON MICROSCOPE

After testing, the soldered specimens, after testing, were cut using a low speed saw with a diamond edged blade, as shown in Figure 8. It was necessary to cut the specimens in order for them to be installed in the specimen holder of the Scanning Electron Microscope (SEM). The SEM used for the analysis was the Zeiss Neon 40 SEM, as shown in Figure 9.

Figure 8. Buehler ISOMET Low Speed Saw

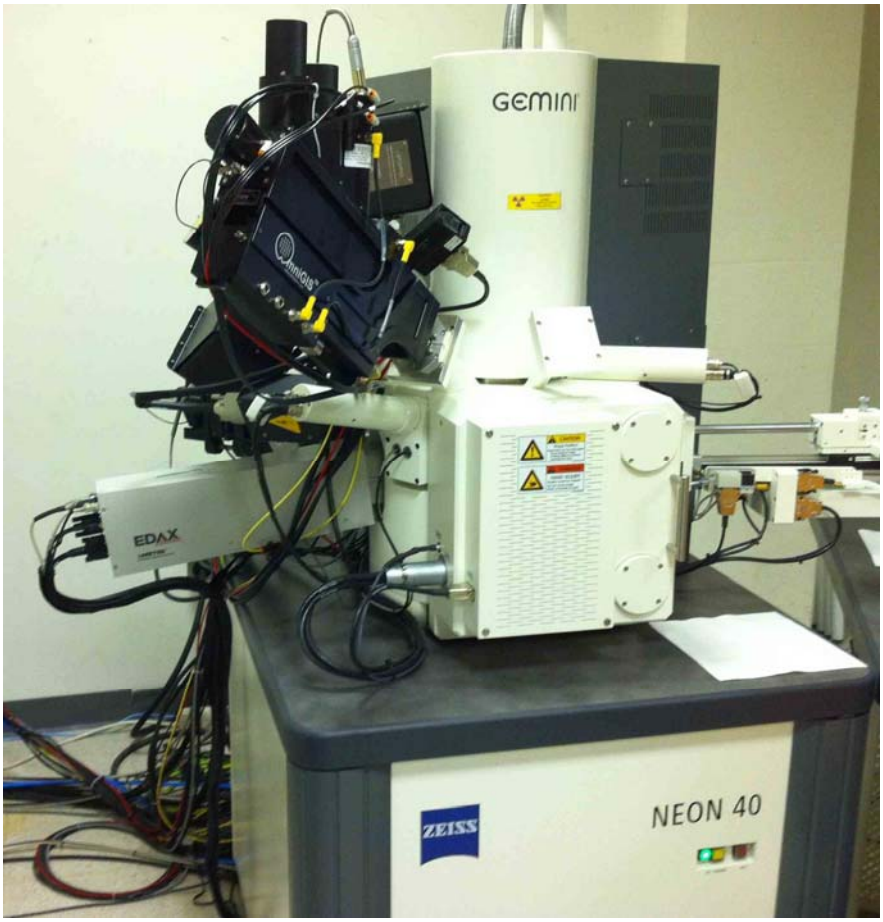

Figure 9. Zeiss Neon 40 SEM

Strain rates of 0.1 s^{-1}, 5.0 s^{-1}, and 10.0 s^{-1} were selected for the SEM, which provided a low, medium, and high strain rate for analysis. The results show that at a strain rate of 0.1 s^{-1}, the solder shows evidence of a bulk solder failure. The two higher strain rates of 5.0 s^{-1} and 10.0 s^{-1}, showed a failure more indicative of an interface failure between the copper and solder. This observation agrees with previous research done by Su *et al.* [4] when using lead-and tin solder.

Figure 10 shows SEM results of strain rate 0.1 s^{-1}. In this figure, the cupping is scattered throughout the interface cross-section, which indicates the presence of excess solder that remained on the copper rod after the axial tension test. The excess solder shows the evidence of a bulk solder failure as the solder fails.

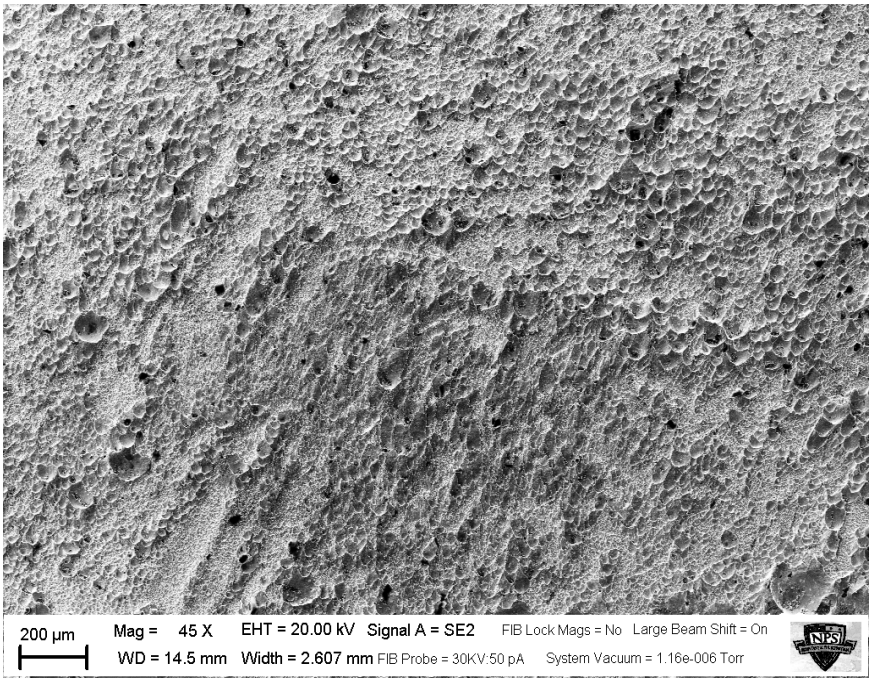

Figure 10. SEM image of strain rate 0.1 s^{-1}

Figure 11 and Figure 12 show the SEM results for strain rates 5.0 s^{-1} and 10.0 s^{-1}. On both figures, flat areas without cupping can be seen and these areas show evidence of an interface failure. The parallel lines seen on the figures are from the sanding of the copper rod during specimen preparation.

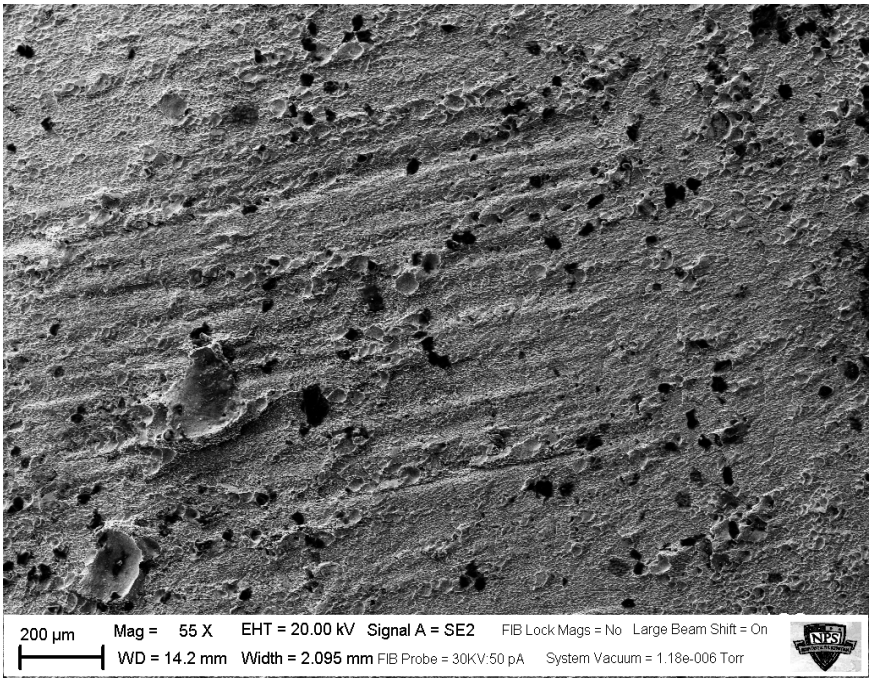

Figure 11. SEM image for strain rate 5.0 s^{-1}

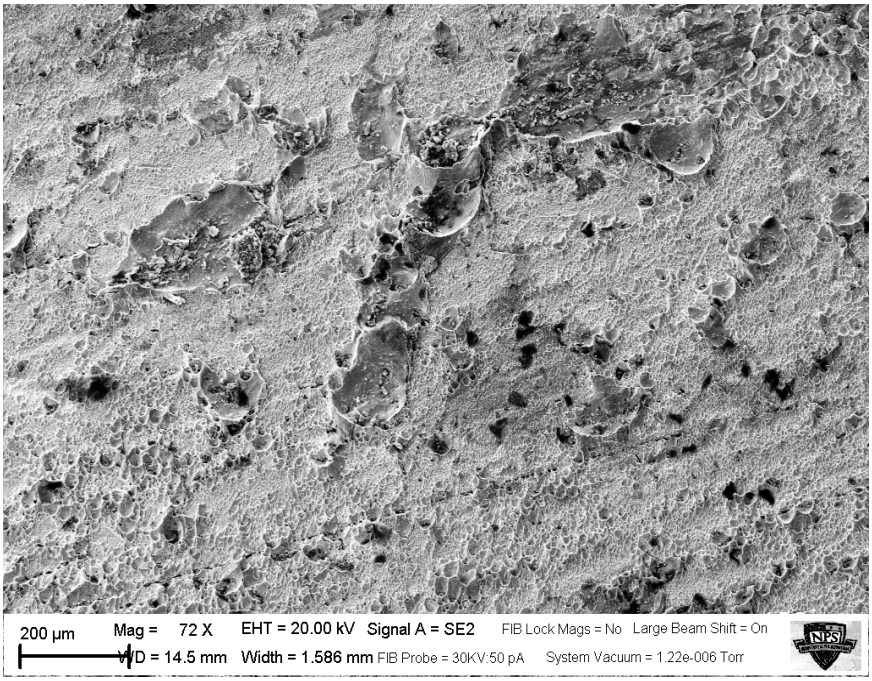

Figure 12. SEM image for strain rate 10.0 s^{-1}

B. FINITE ELEMENT ANALYSIS

A Finite Element (FE) model of the specimen was created using Solidworks 13.0 for the specimen model and this was imported into ANSYS workbench 13.0 for FE analysis.

The FE model was created to show the stress concentrations along the copper solder interface as was well as the stress distribution throughout the specimen. The specimen is not of a traditional dog bone shape normally used in tensile testing to reduce stress concentrations. Therefore, the FE analysis will give insight on the distribution of the stresses in the specimen. Figure 13 shows the specimen modeled before the addition of forces.

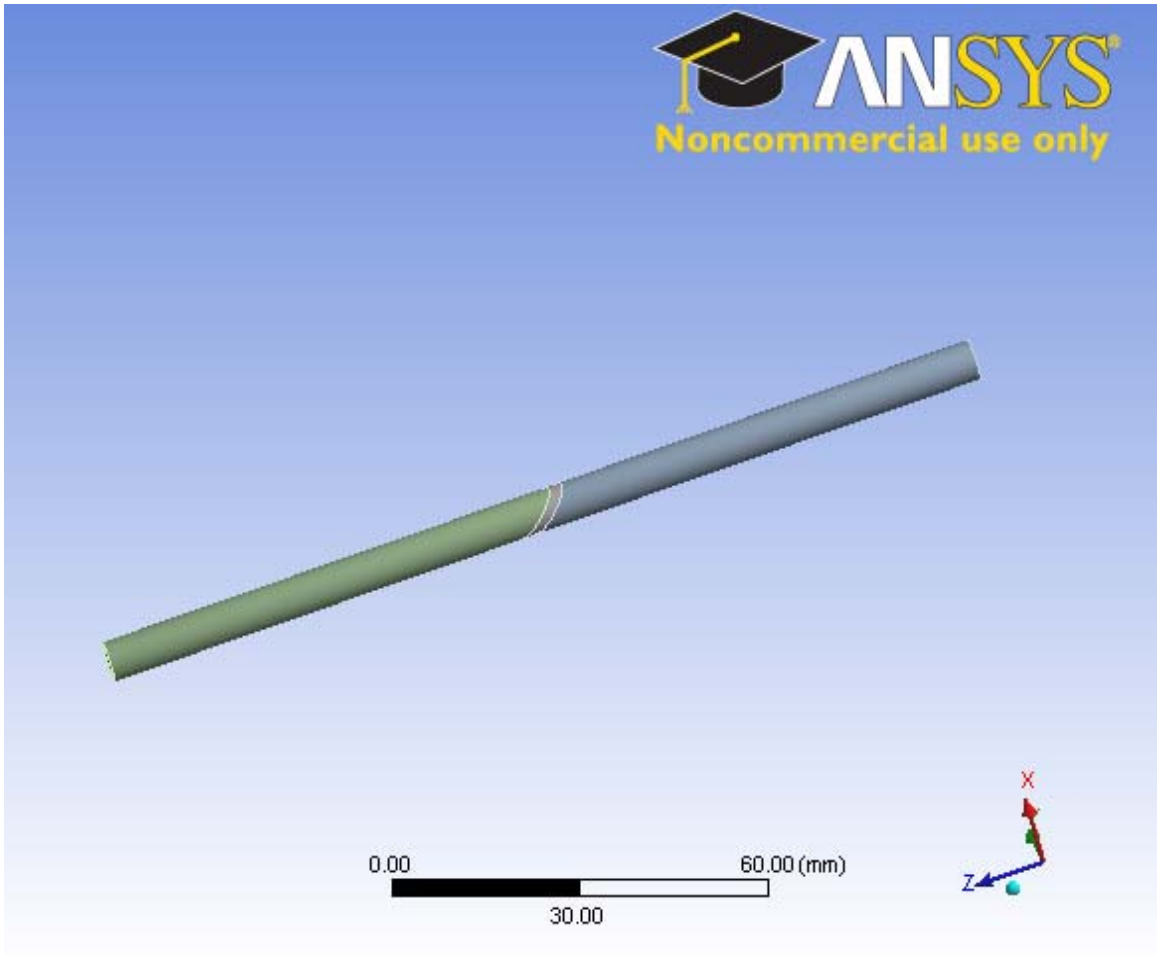

Figure 13. Specimen modeled in ANSYS Workbench and Solidworks.

The FE model was fixed at one end and elongated by 1.0 mm on the opposite end as shown in Figure 14. Figure 15 shows the results of the FE model with the highest stress in the solder and the lowest stresses in the copper along the solder-copper interface.

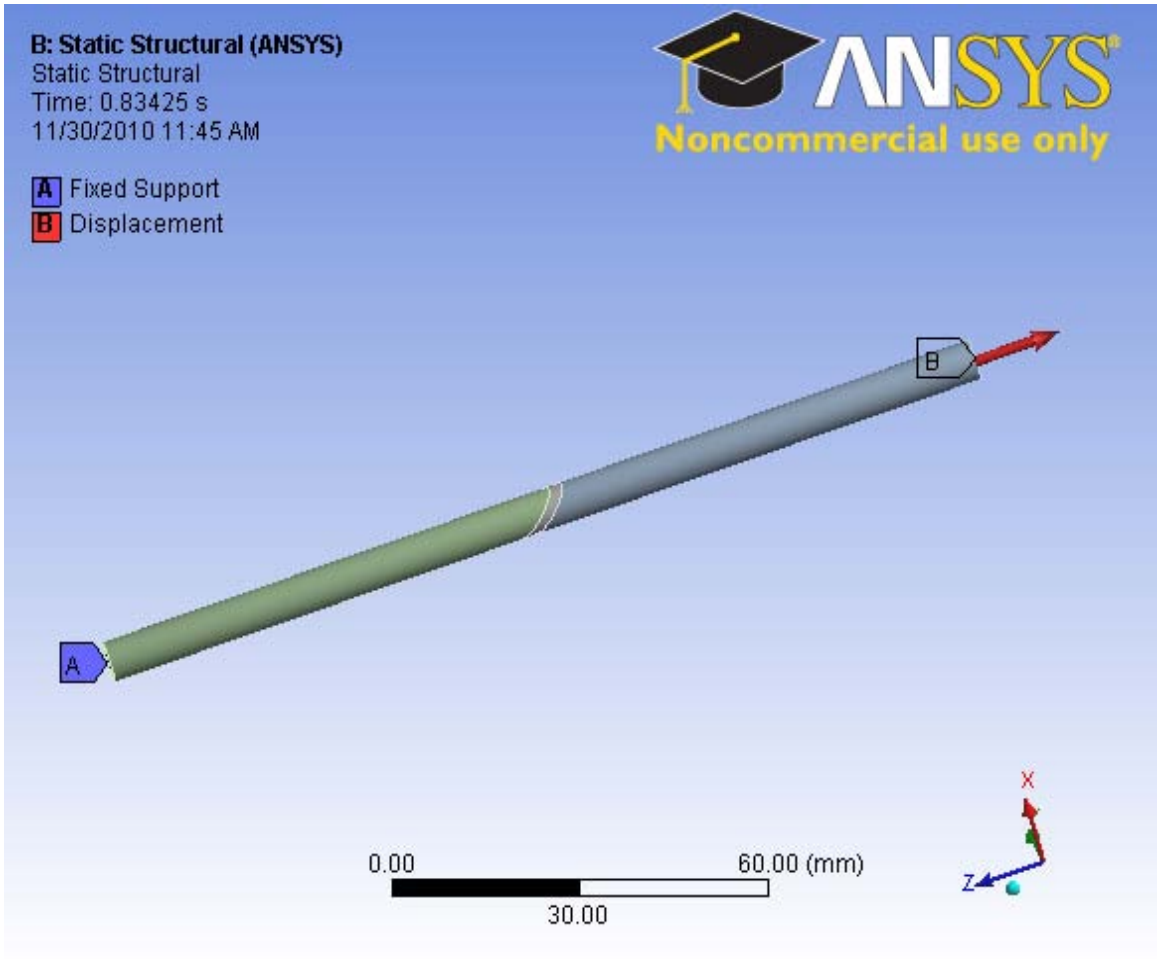

Figure 14. Fixed Support and applied displacement.

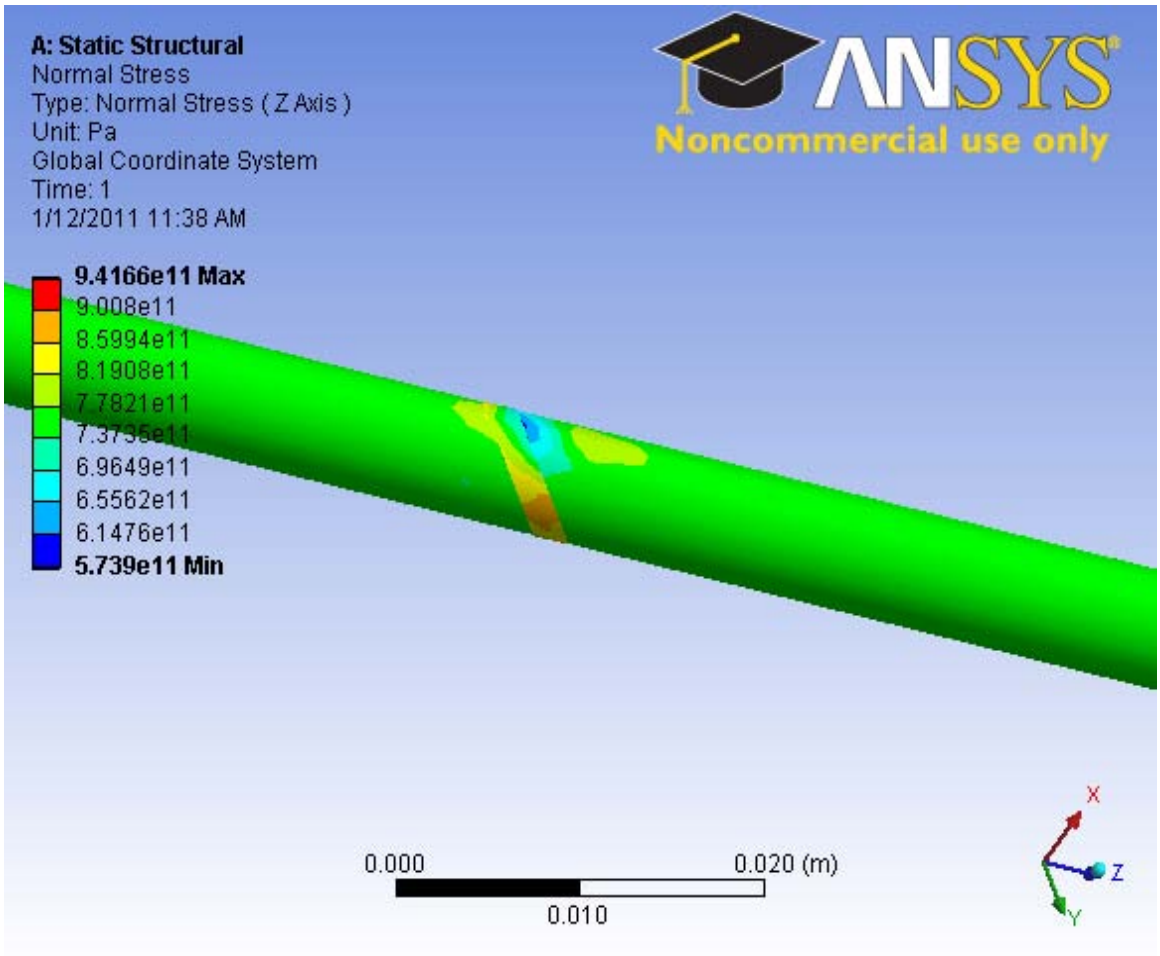

Figure 15. Stress concentration and distribution.

Figure 16 shows a zoomed view of the solder joint to better illustrate the stress concentration and distribution along the solder-copper interface. It can be seen that there are high stresses in the solder and the copper has appreciably less stresses.

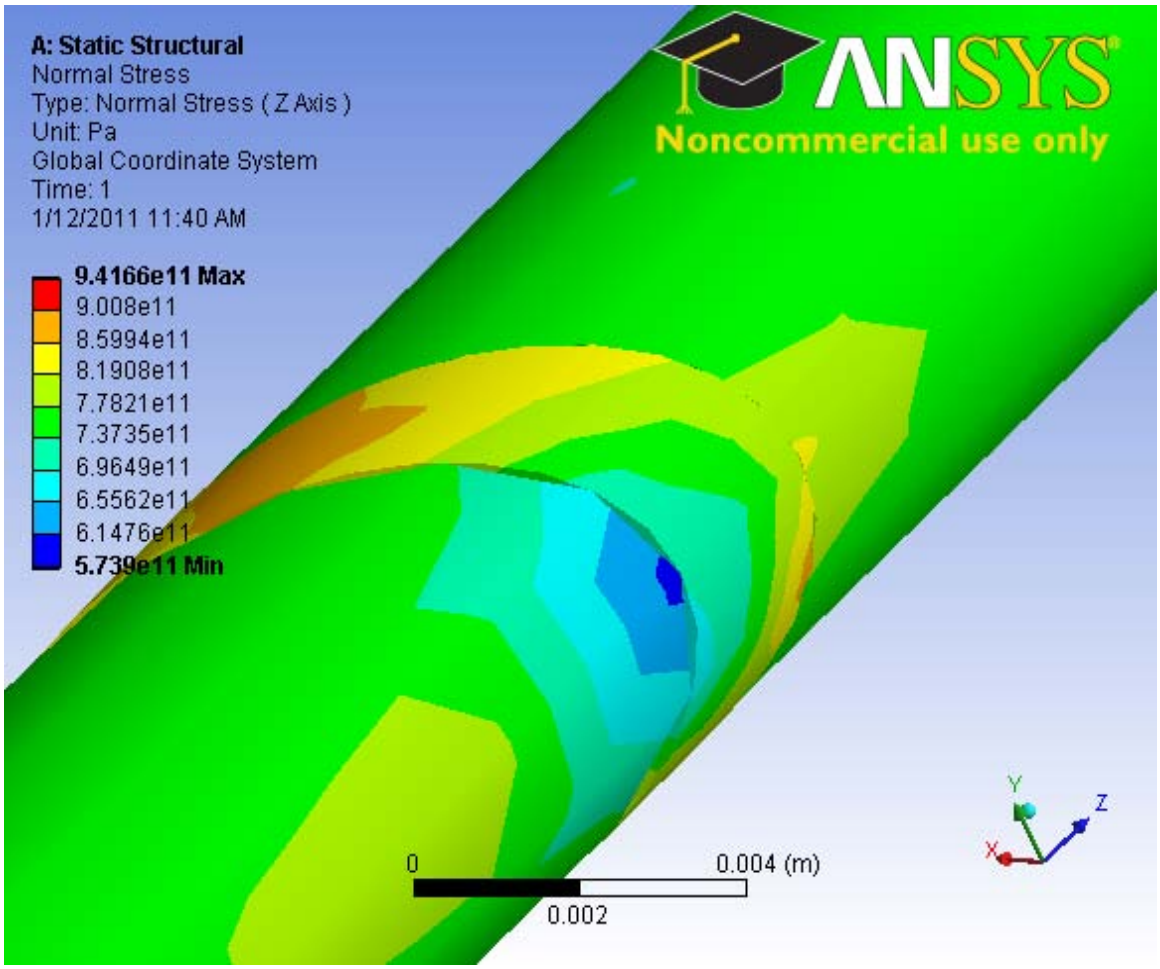

Figure 16. Stress concentration and distribution.

Figure 17 shows a cross-section cut of the solder on the FE model. It can be seen that the stresses are more of less evenly distributed throughout the bulk solder and the majority of the stresses are of the same magnitude as the stresses in the copper.

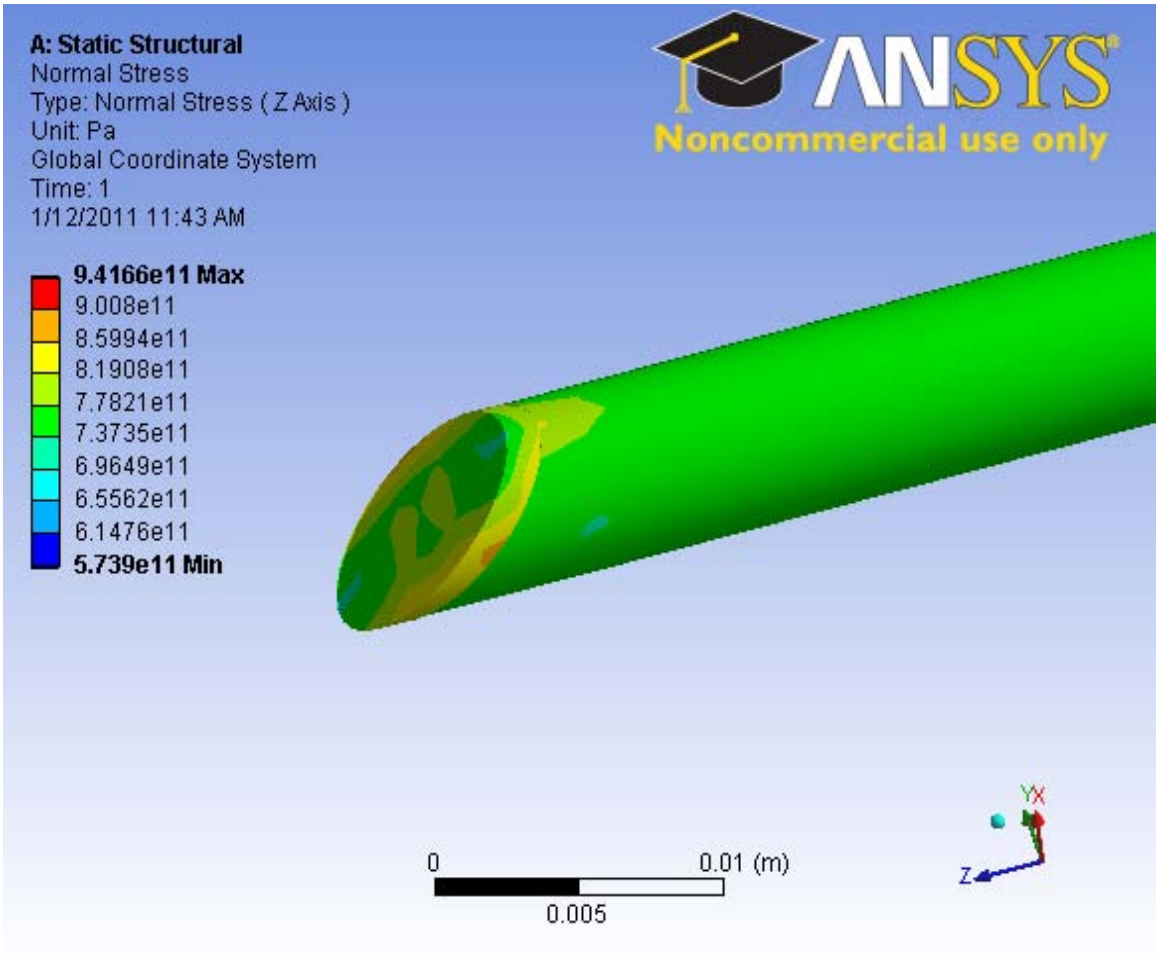

Figure 17. Cross-section view of solder.

C. SINGLE STRAIN RATE RESULTS

The results of the single-strain rate tests at room temperature are included in Table 4.

Table 4. Results of single-strain rate tests at room temperature.

Strain Rate (s^{-1})	0.05	0.1	1.0	5.0	10.0
Modulus (MPa)	3.67	3.44	3.42	2.36	1.72
Max Force Applied (N)	1755.6	2009.9	2520.0	2827.3	2792.2
Yield Stress (kPa)	69.9	89.6	122.6	178.5	224.1
Ultimate Stress (kPa)	176.0	201.5	252.4	283.5	280.3
Failure Stress (kPa)	174.7	196.4	249.5	282.3	279.4
Strain at Yield Strength (kPa)	0.022	0.031	0.045	0.095	0.098
Ultimate Strain (mm/mm)	0.092	0.120	0.118	0.223	0.293
Failure Strain (mm/mm)	0.096	0.132	0.223	0.258	0.314
Total Strain Energy Density (kJ/m^3)	11.2	18.3	42.1	55.6	62.6
Plastic EnergyDensity (kJ/m^3)	7.1	12.4	32.9	38.9	39.9

The yield and ultimate strengths are plotted in Figure 18. Both yield and ultimate strengths increase as the strain rate is increased. The amount of increase in the both yield and ultimate strengths at lower strain rates is much higher than those at higher strain rates. It should be noted that the ultimate strength of strain rate 10.0 s^{-1} is slightly lower than at strain rate of 5.0 s^{-1}. This could indicate that the upper limit of strength has been reached in the solder joint.

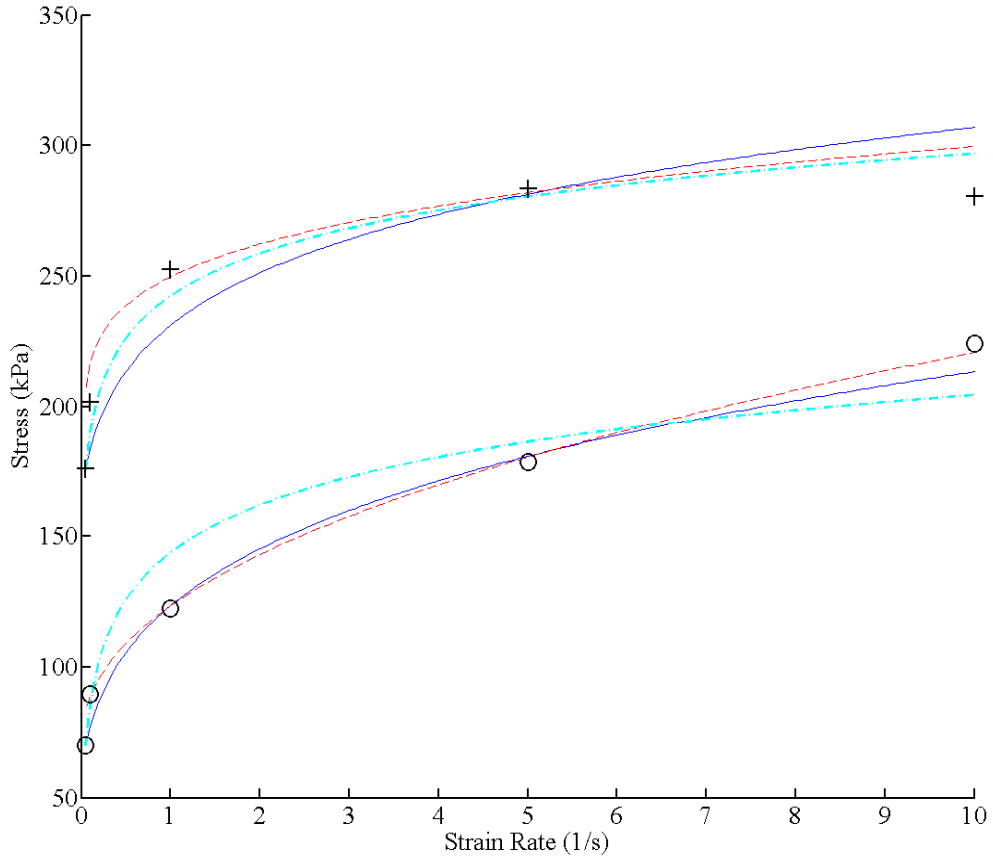

+:Ultimate Strength, O: Yield Strength, Dashed lines fitted to $\theta = \theta_0[1+\left(\frac{\dot{\varepsilon}}{D}\right)^{\frac{1}{q}}]$, Dashed-dotted lines fitted to $\theta = C\log\left(\frac{\dot{\varepsilon}}{\dot{\varepsilon}_0}\right)+\theta_0$ and the solid lines fitted to $\theta = \theta_0\left(\frac{\dot{\varepsilon}}{\dot{\varepsilon}_0}\right)^m$.

Figure 18. Variations of the yield and ultimate strength with strain rate at a room temperature.

The experimental data in Figure 18 were fitted to Equations (2), (3) and (4). The dashed lines in Figure 18 are fitted to Equation (2), dashed-dotted lines to Equation (3) and the solid line to Equation (4).

$$\theta = \theta_0[1 + \left(\frac{\dot{\varepsilon}}{D}\right)^{\frac{1}{q}}] \tag{2}$$

$$\theta = C\log\left(\frac{\dot{\varepsilon}}{\dot{\varepsilon}_0}\right) + \theta_0 \tag{3}$$

$$\theta = \theta_0\left(\frac{\dot{\varepsilon}}{\dot{\varepsilon}_0}\right)^m \tag{4}$$

The ultimate strength constants: q, m, and C were determined to be 4.512, 0.127, and 23.818 respectively. The constant D for ultimate strength was determined to be 147.05 s^{-1}. The yield strength constants: q, m, and C were determined to be 2.223, 0.242, and 26.507 respectively. The constant D for yield strength was determined to be 1.812 s^{-1}.

The base strain rate for this thesis is 0.05 s^{-1} and the base yield and ultimate strengths are 69.92 kPa and 176.00 kPa, respectively. The aforementioned base values are used in Equations (2) – (4) and are their use is denoted by the subscript '0.'

The strain at fracture, ultimate load, and yield are plotted against strain rate in Figure 19. This gives a good illustration on how the fracture strains grow linearly on the logarithmic plot. The logarithmic plot gives good resolution to what is happening at the lower strain rates. It should be noted that at a strain rate of 1.0 s^{-1}, the amount of strain between the ultimate load and fracture is larger than compared to any other strain rate. For all the other strain rates the strain at ultimate load and fracture are relatively close.

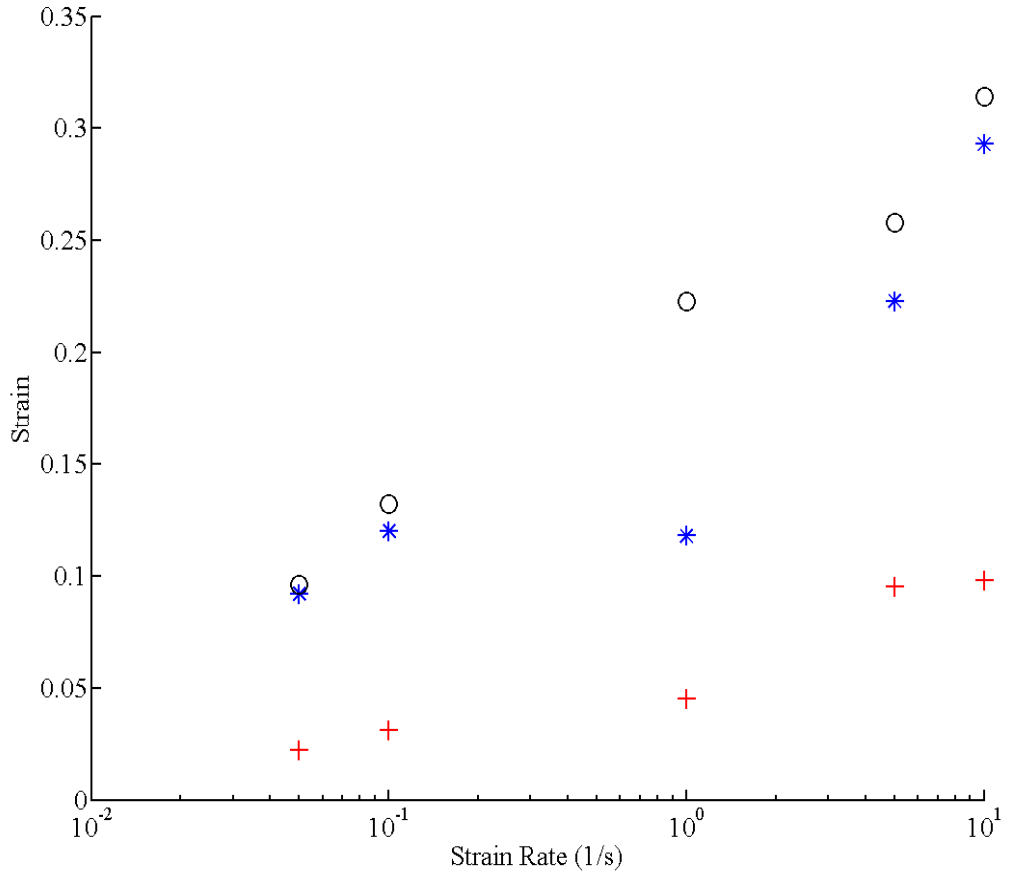

O: Strain at fracture; *: Strain at ultimate load; +: Strain at yield

Figure 19. Variations with strain rate of the strains at fracture, ultimate load, and yield under a room temperature.

The elastic modulus is plotted against the logarithmic strain rate in Figure 20. The figure clearly shows that modulus rapidly drops after strain rate 1.0 s^{-1} and takes a linear trend in the negative direction. For strain rates below 1.0 s^{-1}, the elastic modulii are relatively constant.

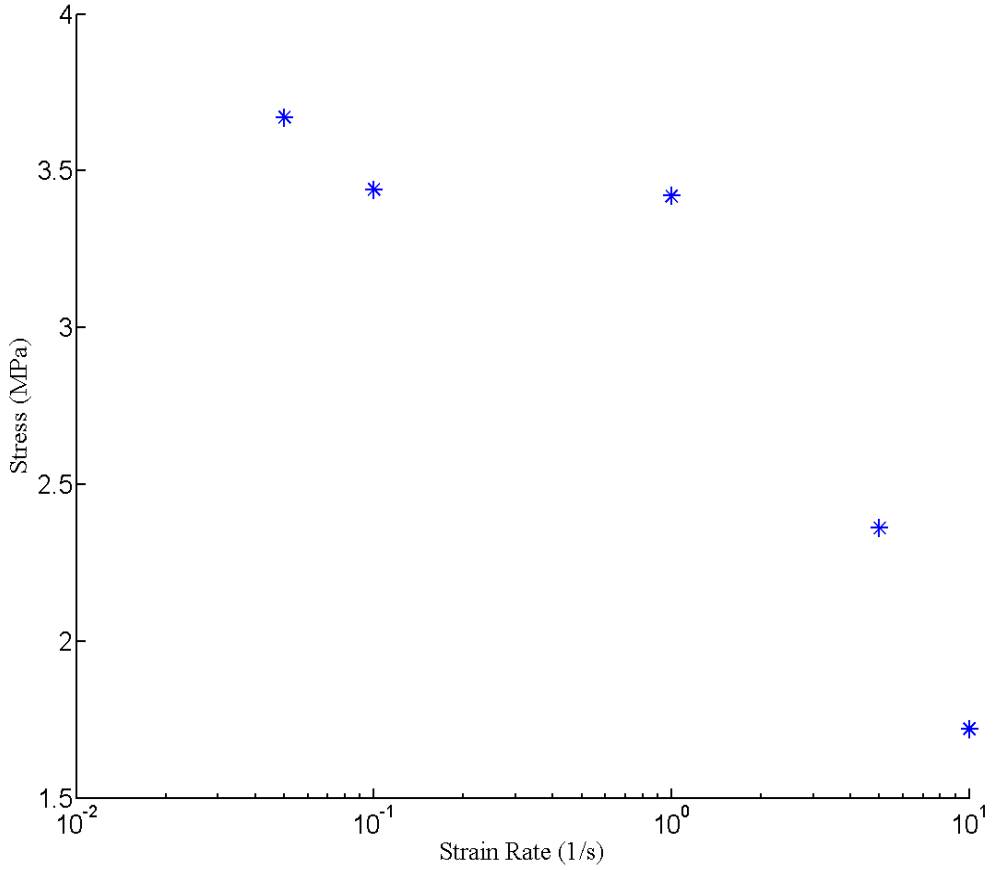

Figure 20. Variation of elastic modulus with strain rate.

D. SINGLE STRAIN RATE RESULTS WITH SPECIMEN HEATING

The strain rates of 0.05 s^{-1}, 1.0 s^{-1}, and 10.0 s^{-1} were chosen for testing the effects of the specimens at a temperature of 65.5 degrees Celsius, which represents a temperature under operating conditions. The test data for the heated specimens are included in Table 5.

Table 5. Results of single-strain rate tests with heated specimens.

Strain Rate (s^{-1})	0.05	1.0	10.0
Elastic Modulus (MPa)	3.73	2.90	1.08
Maximum Force (N)	1654.2	2095.0	1664.2
Yield Stress (kPa)	73.9	115.1	136.8
Ultimate Stress (kPa)	165.8	210.0	166.9
Strain at Yield Strength	0.022	0.046	0.175
Ultimate Strain (mm/mm)	0.105	0.157	0.294
Failure Strain (mm/mm)	0.124	0.199	0.294
Total Strain Energy Density (kJ/m^3)	15.5	31.5	27.3
Plastic EnergyDensity (kJ/m^3)	12.2	23.9	15.3

The elastic modulus of the heated and non-heated specimens are plotted in Figure 21 for comparison and shows a difference between them. A similarity between the heated and non-heated specimens is as the strain rate increased, the elastic modulus decreased. It should be noted that the elastic modulus of strain rate 0.05 s^{-1} of the heated specimen is slightly higher than the elastic modulus of the non-heated specimen at the same strain rate. The remaining heated test specimens had a lower elastic modulus as compared to the non-heated specimens.

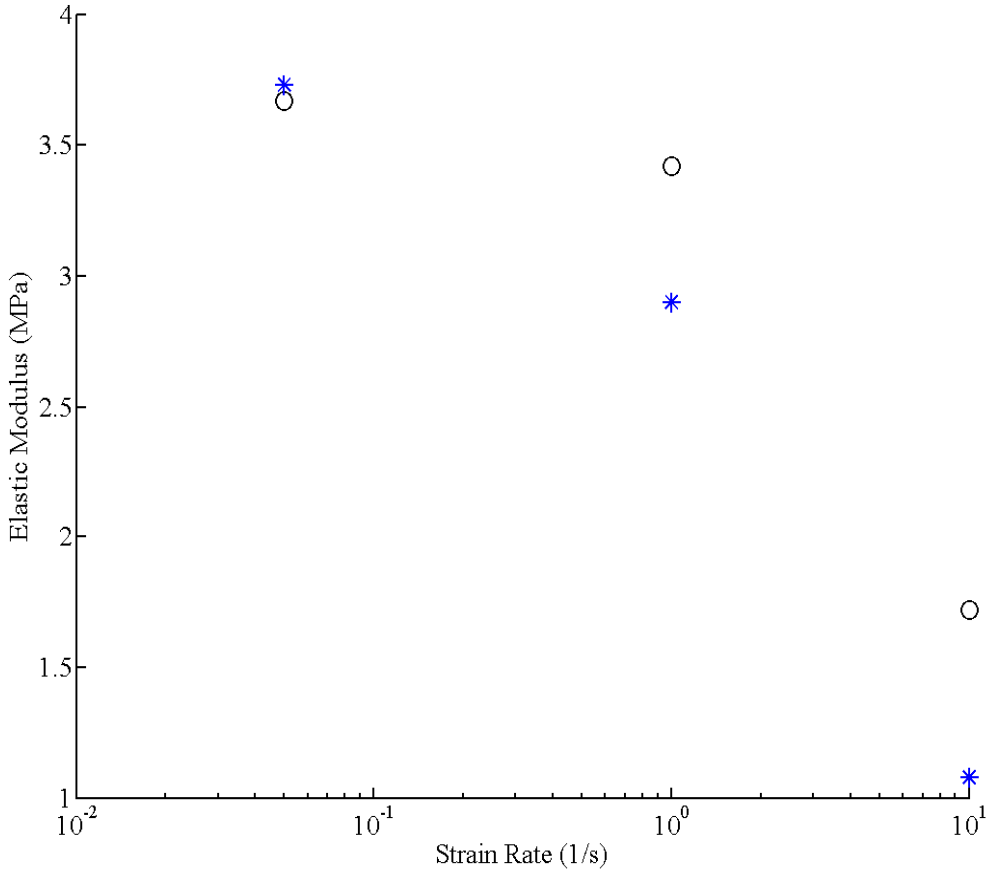

*: Elastic modulus of heated specimens, O: Elastic modulus of non-heated specimens

Figure 21. Comparison of elastic modulii of heated and non-heated specimens.

The ultimate strengths of the heated and non-heated specimens are plotted in Figure 22. As predicted, the ultimate strength of the heated specimens is lower than that of the non-heated specimens.

The yield strengths of the heated and non-heated specimens are plotted in Figure 23. Comparing the yield strengths, the strain rate of 0.05 s^{-1} has a slightly higher yield strength than that of the non-heated specimen. In both figures, the difference between the heated and non-heated strengths increases with an increase in the strain rate. It should be noted that for the highest strain rate of 10.0 s^{-1}, the strength of the heated specimen was roughly half of the non-heated specimen.

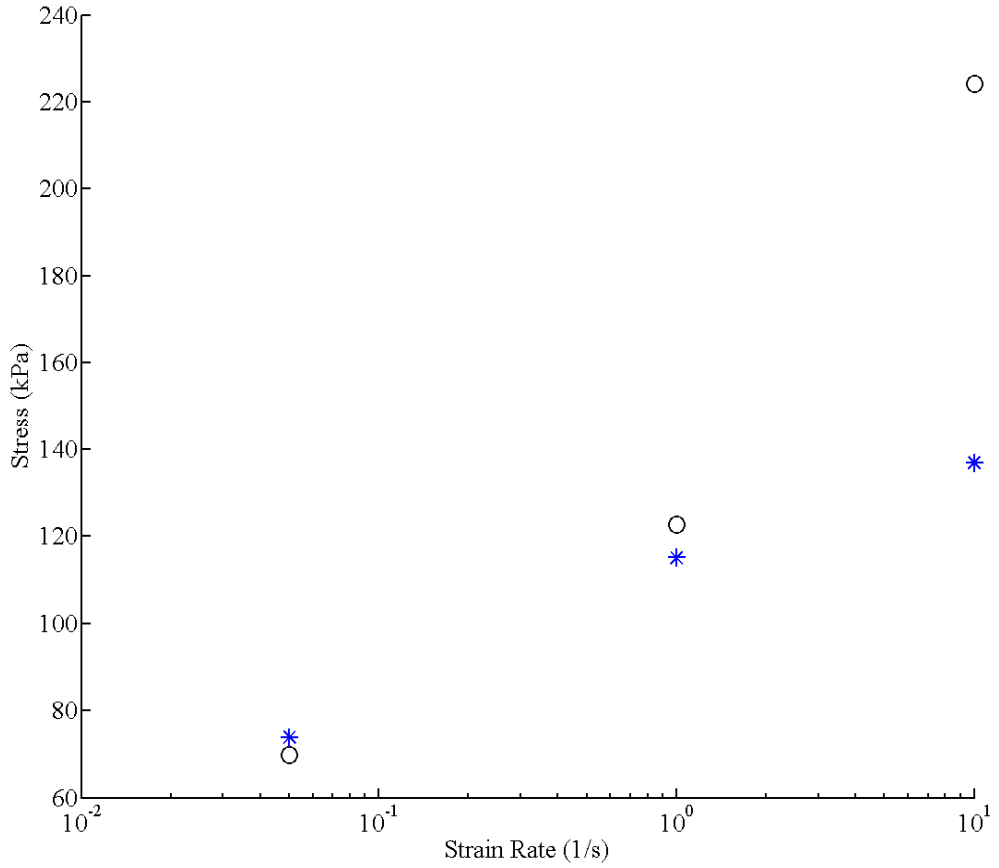

*: Ultimate strength of heated specimens, O: Ultimate strength of non-heated specimens

Figure 22. Comparison of ultimate strengths of heated and non-heated specimens.

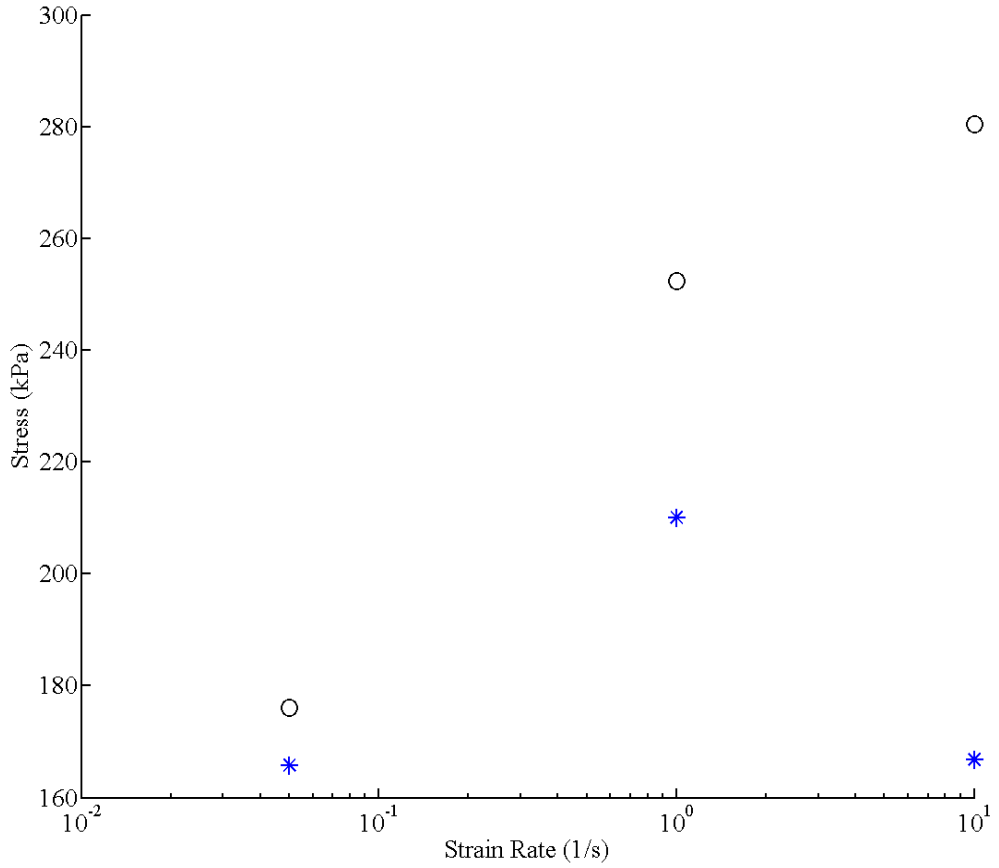

*: Yield strength of heated specimens, O: Yield strength of non-heated specimens

Figure 23. Comparison of yield strengths of heated and non-heated specimens.

The strains at fracture, ultimate load, and yield are plotted against strain rate in Figure 24. This gives a good illustration on how similar the fracture strains are as compared to the fracture strains of the non-heated specimens in Figure 19. The fracture strains of the heated specimens follow a near linear growth on the logarithmic plot.

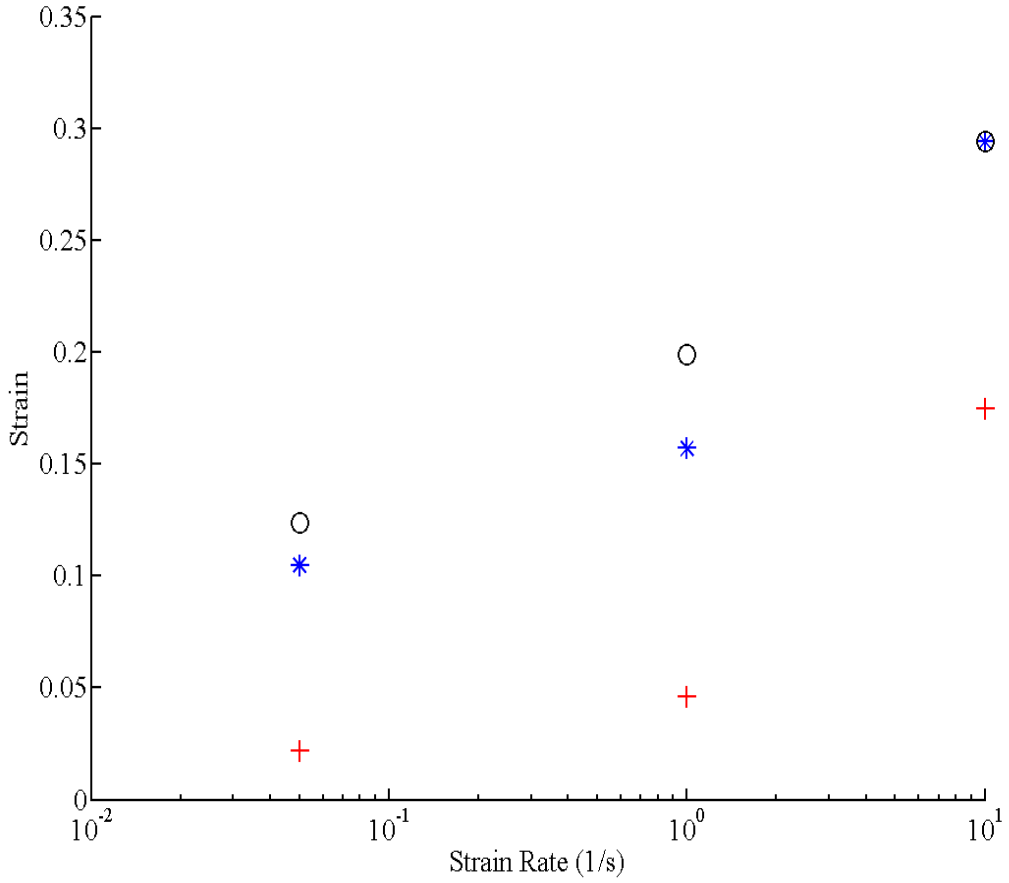

O: Strain at fracture; *: Strain at ultimate load; +: Strain at yield

Figure 24. Variations with strain rate of the strains at fracture, ultimate load, and yield for heated specimens.

A few points of interest should be noted when comparing the strains of the heated and non-heated specimens. The strain at yielding for both 0.05 s^{-1} and 1.0 s^{-1} were the same magnitude for the heated and non-heated specimens. Additionally, the fracture and ultimate strains for strain rate 10.0 s^{-1} are the same magnitude. The fracture strain at strain rate 0.05 s^{-1} at fracture was higher for the heated specimen than for the non-heated specimens, but this was not the case for the other two strain rates. Fracture strains for the heated and non-heated specimens are shown in Figure 25. It is expected that as the specimen is heated, it can withstand a lesser amount of stress but the fracture strain becomes larger with more ductility.

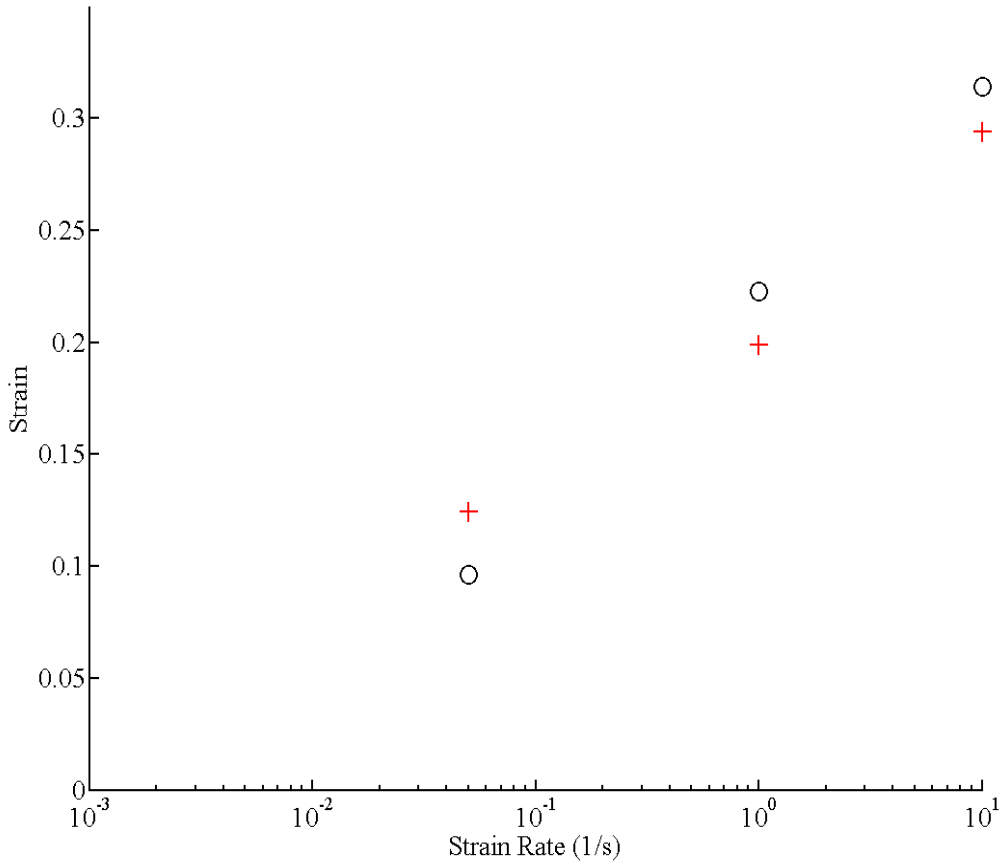

+: Heated specimen fracture strain, O: Non-heated specimen fracture strain

Figure 25. Fracture strain comparison of heated and non-heated specimens.

Figure 26 shows a stress-strain curve comparing the heated and non-heated specimens at two strain rates, 1.0 s^{-1} and 0.05 s^{-1}. From the figure, it can be seen that the ultimate strength of the heated specimens are lower than the non-heated specimens. Also note, the fracture strain of the heated specimens lie in between the fracture strains of the non-heated specimens.

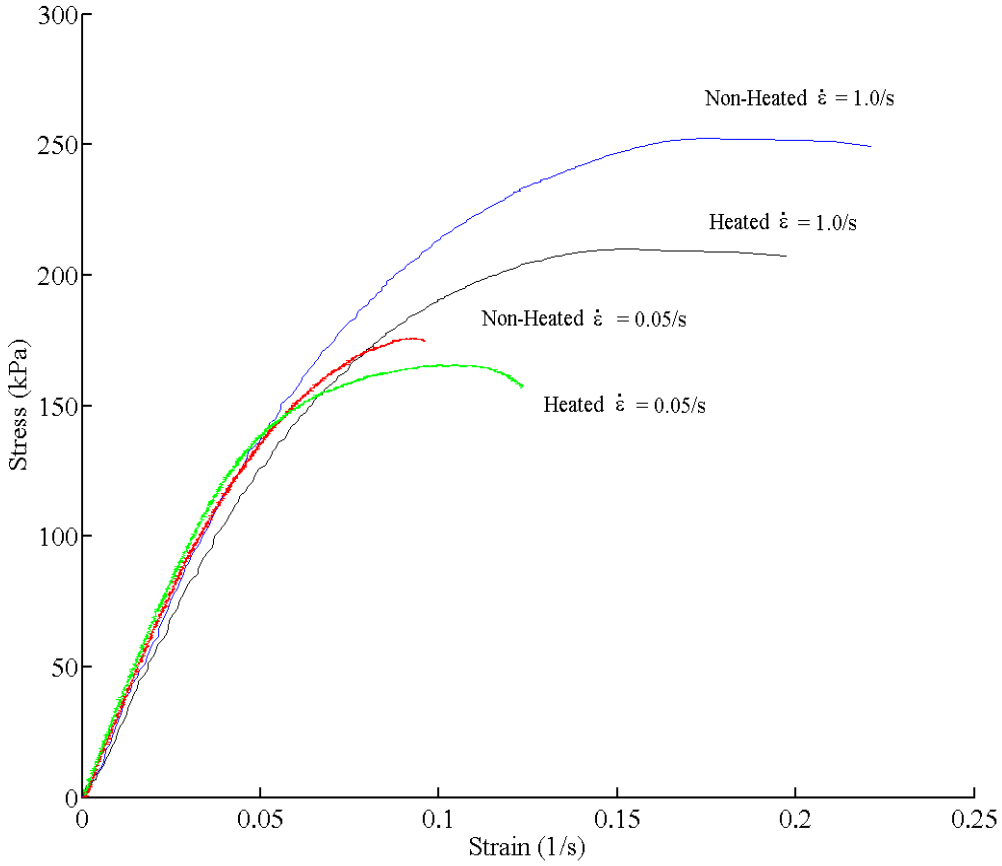

Figure 26. Comparison of heated and non-heated single-rate specimens.

E. MULTIPLE STRAIN RATE RESULTS

Chapter II outlined the parameters at which the 12 multiple strain rate tests were performed on the specimens.

Tables 6 and 7 show the results of the specimens at room temperature as they were subjected to varying strain rates before and after yield strength of the initial strain rate curve, respectively. The tests were performed with an initial strain rate of 1.0 s^{-1} transitioning to a strain rate of 0.05 s^{-1} until failure of the solder joint.

Table 6. Multiple strain rate results of strain rates 1.0 s^{-1} to 0.05 s^{-1} before yield strength of the initial strain rate for unheated specimens.

Transition Strain (mm/mm)	0.016	0.020	0.027
Elastic Modulus (MPa)	3.13	3.13	3.13
Maximum Force (N)	1974.6	2117.3	1828.3
Ultimate Stress (kPa)	197.9	212.3	183.3
Failure Stress (kPa)	191.1	201.1	175.8
Ultimate Strain (mm/mm)	0.115	0.127	0.097
Failure Strain (mm/mm)	0.126	0.149	0.131
Total Strain Energy Density (kJ/m^3)	17.3	20.3	17.9
Plastic Energy Density (kJ/m^3)	11.1	13.7	12.7
Total Strain Energy Density for 1.0 (kJ/m^3)	0.068	0.604	1.3
Total Strain Energy Density for 0.05 (kJ/m^3)	17.3	19.6	10.0

Table 7. Multiple strain rate results of strain rates 1.0 s^{-1} to 0.05 s^{-1} after yield strength of the initial strain rate for unheated specimens.

Transition Strain (mm/mm)	0.047	0.057	0.072
Elastic Modulus (MPa)	3.13	3.13	3.13
Maximum Force (N)	1944.5	1929.0	2099.6
Ultimate Stress (kPa)	192.1	193.4	210.5
Failure Stress (kPa)	188.5	186.1	209.3
Ultimate Strain (mm/mm)	0.099	0.121	0.136
Failure Strain (mm/mm)	0.106	0.148	0.148
Total Strain Energy Density (kJ/m^3)	13.2	23.0	21.4
Plastic Energy Density (kJ/m^3)	8.5	17.8	13.2
Total Strain Energy Density for 1.0 (kJ/m^3)	3.0	6.6	5.4
Total Strain Energy Density for 0.05 (kJ/m^3)	10.1	11.6	9.0

Figure 27 shows a typical stress-strain curve for a specimen subjected to a varying strain rate with an initial strain rate of 1.0 s^{-1} and a second strain rate of 0.05 s^{-1}. Included in the figure are the results of the specimens when subjected to single strain rates of 1.0 s^{-1} and 0.05 s^{-1}. It should be noted that the elastic modulus of the specimen subjected to a varying strain rate is the same as the elastic modulus of the initial strain rate to which the specimen is subjected.

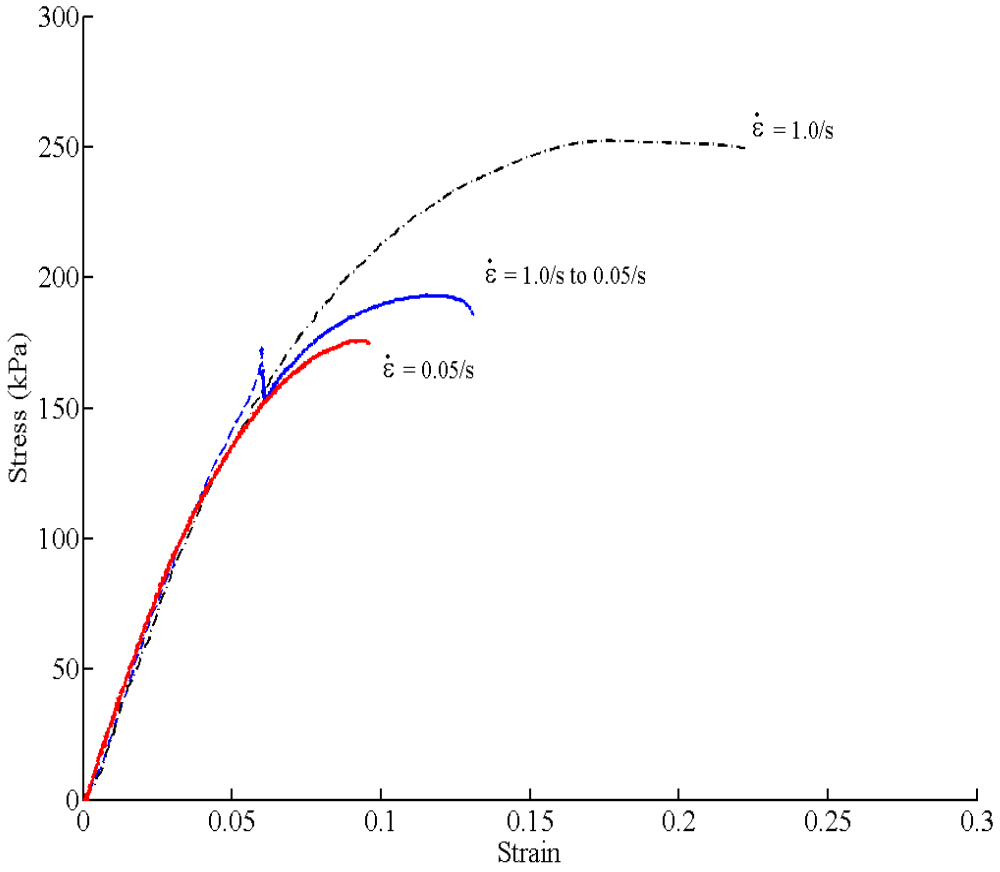

Figure 27. Typical stress-strain curve under two strain rates at room temperature.

Tables 8 and 9 show the results of the specimens that were subjected to varying strain rates before and after yield stress, respectively when the strain rates are reversed. The tests were performed at room temperature with an initial strain rate of 0.05 s^{-1} transitioning to a strain rate of 1.0 s^{-1} until failure of the solder joint.

Table 8. Multiple strain rate results of strain rates 0.05 s^{-1} to 1.0 s^{-1} before yield strength of the initial strain rate for unheated specimens.

Transition Strain (mm/mm)	0.010	0.016	0.024
Modulus (MPa)	3.27	3.27	3.27
Maximum Force (N)	2582.4	2279.7	2653.5
Ultimate Stress (kPa)	258.9	228.6	296.1
Failure Stress (kPa)	258.5	223.4	296.1
Ultimate Strain (mm/mm)	0.181	0.181	0.194
Failure Strain (mm/mm)	0.186	0.196	0.194
Total Strain Energy Density (kJ/m^3)	36.6	33.6	37.5
Plastic Energy Density (kJ/m^3)	25.1	25.5	23.5
Total Strain Energy Density for 0.05 (kJ/m^3)	0.07	0.48	0.42
Total Strain Energy Density for 1.0 (kJ/m^3)	41.1	33.0	27.3

Table 9. Multiple strain rate results of strain rates 0.05 s^{-1} to 1.0 s^{-1} after yield strength of the initial strain rate for unheated specimens.

Transition Strain (mm/mm)	0.031	0.042	0.057
Modulus (MPa)	3.27	3.27	3.27
Maximum Force (N)	2659.8	2416.5	2470.7
Ultimate Stress (kPa)	266.6	242.2	247.7
Failure Stress (kPa)	266.7	242.3	247.7
Ultimate Strain (mm/mm)	0.157	0.157	0.154
Failure Strain (mm/mm)	0.157	0.157	0.154
Total Strain Energy Density (kJ/m^3)	29.9	24.9	23.9
Plastic Energy Density (kJ/m^3)	14.9	14.9	14.1
Total Strain Energy Density for 0.05 (kJ/m^3)	1.0	2.3	4.3
Total Strain Energy Density for 1.0 (kJ/m^3)	25.1	22.7	19.6

A note to be made is the fracture strains, ultimate strength and total strain energy densities for specimens subjected to an initial fast strain rate followed by a slow strain rate are much greater than when the strain rates are reversed.

Figure 28 shows a typical stress-strain curve for a specimen subjected to a varying strain rate with an initial strain rate of 0.05 s^{-1} and a second strain rate of 1.0 s^{-1}. Included in the figure are the results of the specimens when subjected to single strain rates of 1.0 s^{-1} and 0.05 s^{-1}. It should be noted as in the first multiple-strain rate test, the elastic modulus of the specimen subjected to a varying strain rate is the same as the elastic modulus of the initial strain rate to which the specimen is subjected.

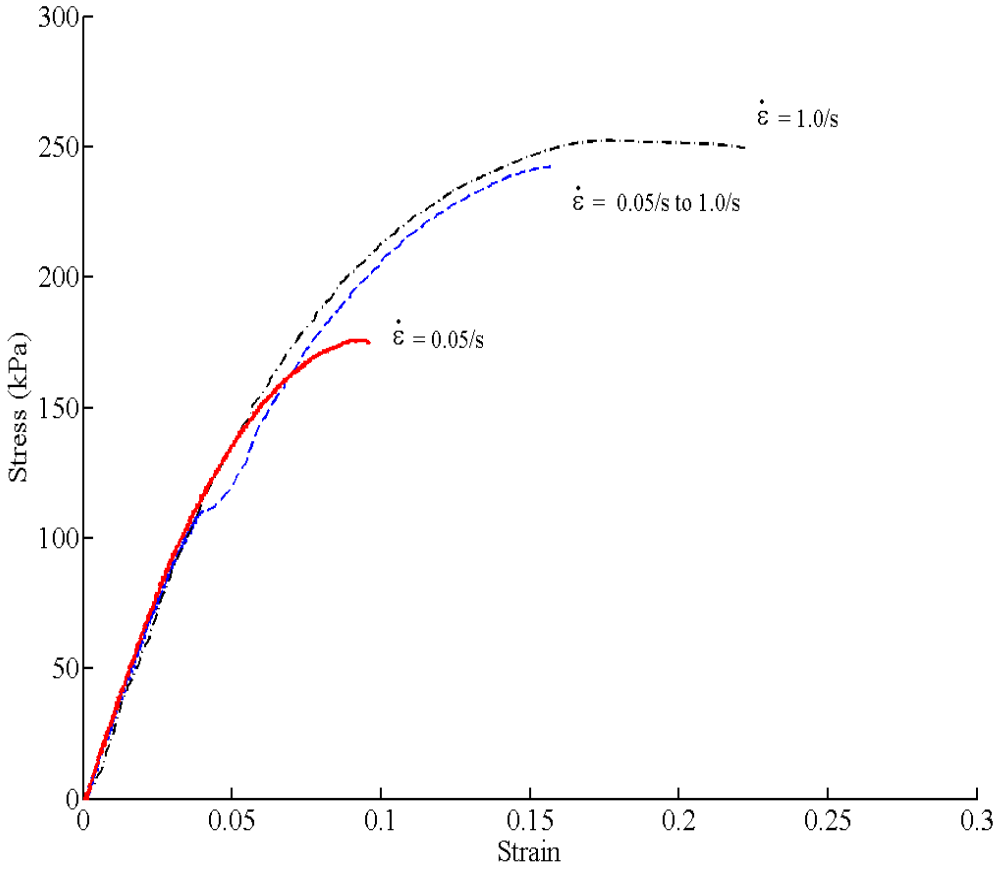

Figure 28. Typical stress-strain curve under two strain rates.

An important observation of the varying strain rate testing was the fracture strain and total shear energy density on all the specimens were between the fracture strain and total shear energy density of the initial and final single-strain rate. These observations are presented in Figures 29 and 30. The data points for the two varying strain rates are averages of the fracture strains and total shear energy densities.

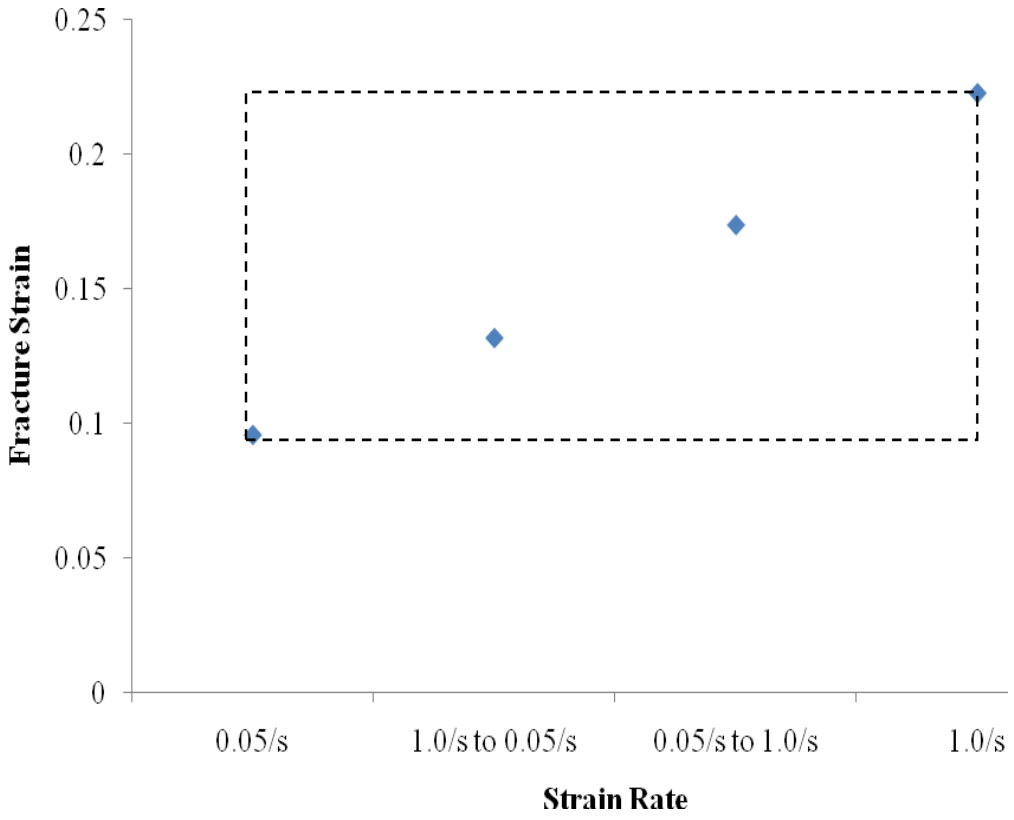

Figure 29. Fracture strain of single and multiple strain rates at room temperature.

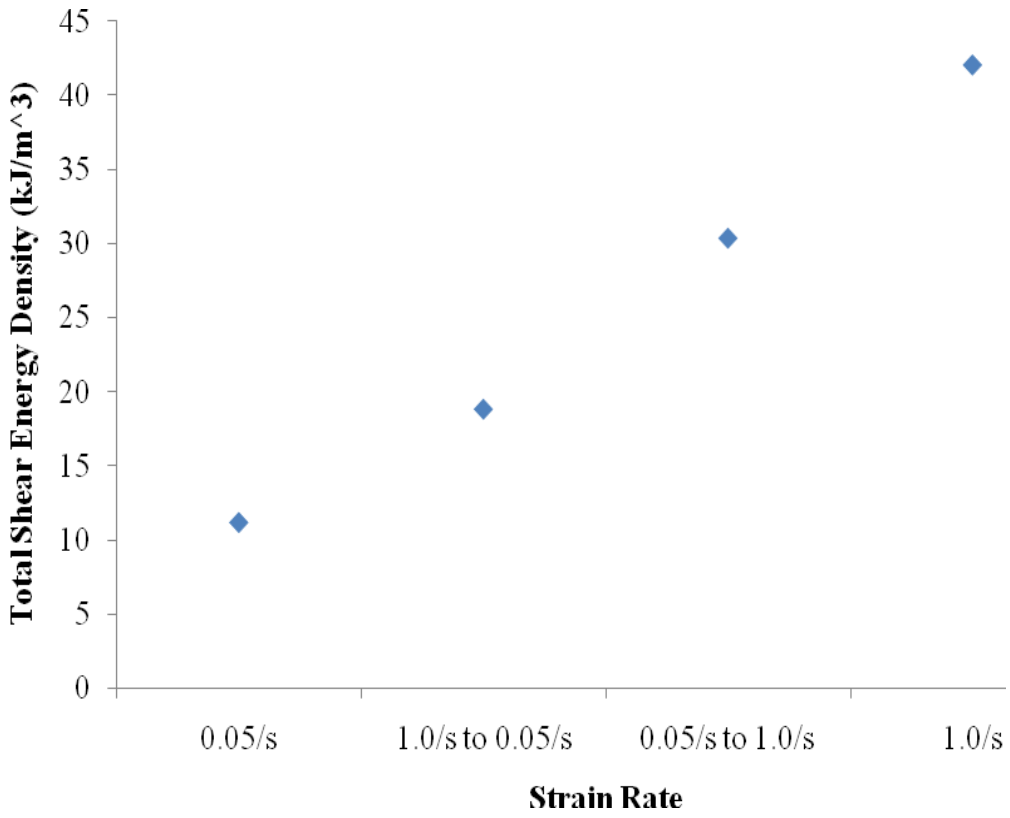

Figure 30. Total Shear Energy Density of single and multiple strain rates.

F. MULTIPLE STRAIN RATE RESULTS WITH SPECIMEN HEATING

The specimens were subjected to the same multiple-strain rates as outlined in Chapter II and the twelve axial tests were performed with the specimens heated to 65.5 degrees Celsius. Tables 10 and 11 shows the results of the specimens as they were subject to varying strain rates before and after yield strength, respectively. The tests were performed with an initial strain rate of 1.0 s^{-1} transitioning to a strain rate of 0.05 s^{-1} until failure of the solder joint.

Table 10. Multiple strain rate results of strain rates 1.0 s^{-1} to 0.05 s^{-1} before yield strength with heating.

Transition Strain (mm/mm)	0.016	0.020	0.027
Elastic Modulus (MPa)	2.90	2.90	2.90
Maximum Force (N)	1287.4	1854.6	1571.9
Ultimate Stress (kPa)	129.1	185.9	157.6
Failure Stress (kPa)	118.9	181.2	141.8
Ultimate Strain (mm/mm)	0.130	0.135	0.122
Failure Strain (mm/mm)	0.163	0.166	0.148
Total Strain Energy Density (kJ/m^3)	17.5	20.4	18.15
Plastic Energy Density (kJ/m^3)	15.1	15.1	14.3
Total Strain Energy Density for 1.0 (kJ/m^3)	0.313	0.421	0.768
Total Strain Energy Density for 0.05 (kJ/m^3)	17.4	20.2	14.8

Table 11. Multiple strain rate results of strain rates 1.0 s^{-1} to 0.05 s^{-1} after yield strength with heating.

Transition Strain (mm/mm)	0.047	0.057	0.072
Elastic Modulus (MPa)	2.90	2.90	2.90
Maximum Force (N)	1785.5	1785.2	1781.9
Ultimate Stress (kPa)	179.0	178.9	178.6
Failure Stress (kPa)	163.4	159.0	153.9
Ultimate Strain (mm/mm)	0.124	0.117	0.125
Failure Strain (mm/mm)	0.165	0.155	0.175
Total Strain Energy Density (kJ/m^3)	23.0	20.6	24.1
Plastic Energy Density (kJ/m^3)	19.9	16.1	20.7
Total Strain Energy Density for 1.0 (kJ/m^3)	2.3	2.7	4.4
Total Strain Energy Density for 0.05 (kJ/m^3)	14.0	16.4	19.5

Figure 31 shows a typical stress-strain curve for a heated specimen subjected to a varying strain rate with an initial strain rate of 1.0 s^{-1} and a second strain rate of 0.05 s^{-1}. Included in the figure are the results of the heated specimens when subjected to single strain rates of 1.0 s^{-1} and 0.05 s^{-1}.

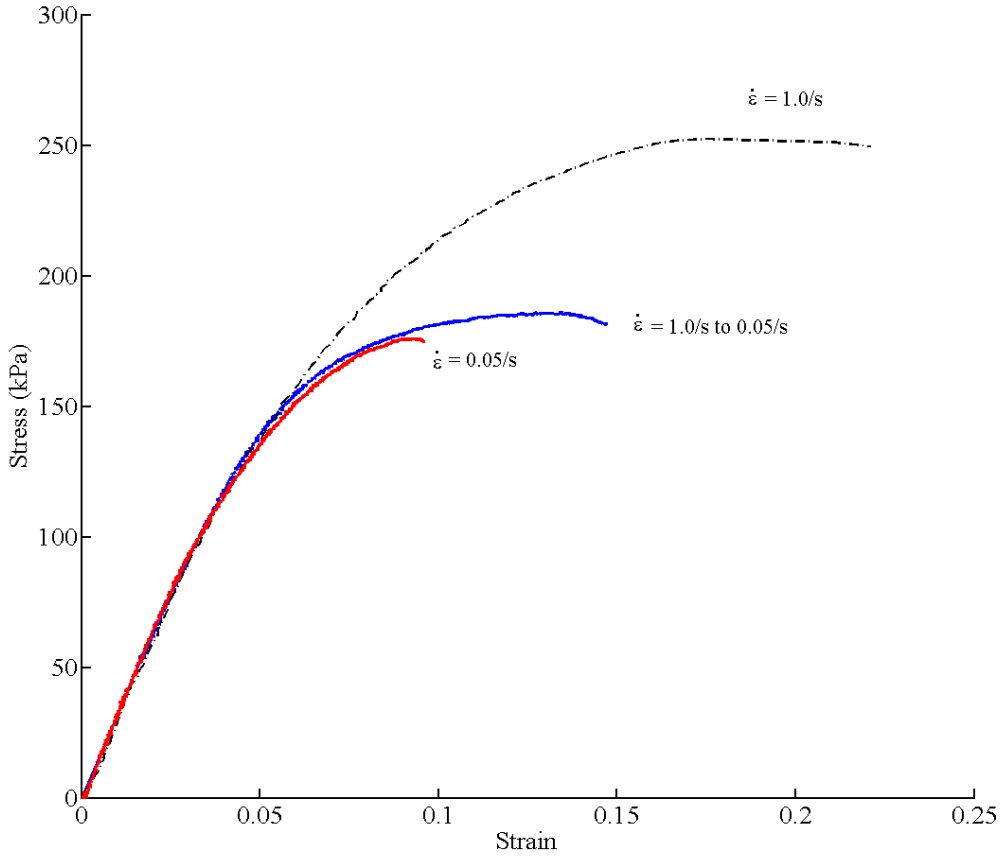

Figure 31. Varying strain rate results of heated specimen.

Tables 12 and 13 show the results of the heated specimens that were subjected to varying strain rates before and after yield strength, respectively. The tests were performed with an initial strain rate of 0.05 s^{-1} transitioning to a strain rate of 1.0 s^{-1} until failure of the solder joint.

Table 12. Multiple strain rate results of strain rates 0.05 s^{-1} to 1.0 s^{-1} before yield strength with heating.

Transition Strain (mm/mm)	0.010	0.016	0.024
Elastic Modulus (MPa)	3.73	3.73	3.73
Maximum Force (N)	2204.5	2397.9	2368.9
Ultimate Stress (kPa)	221.0	240.4	237.5
Failure Stress (kPa)	214.0	238.6	232.3
Ultimate Strain (mm/mm)	0.167	0.139	0.144
Failure Strain (mm/mm)	0.184	0.148	0.170
Total Strain Energy Density (kJ/m^3)	31.4	27.5	29.1
Plastic Energy Density (kJ/m^3)	23.5	18.8	10.9
Total Strain Energy Density for 1.0 (kJ/m^3)	0.07	0.26	0.27
Total Strain Energy Density for 0.05 (kJ/m^3)	31.3	27.2	25.8

Table 13. Multiple strain rate results of strain rates 0.05 s^{-1} to 1.0 s^{-1} after yield strength with heating.

Transition Strain (mm/mm)	0.031	0.042	0.057
Elastic Modulus (MPa)	3.73	3.73	3.73
Maximum Force (N)	2022.3	2739.0	2106.6
Ultimate Stress (kPa)	198.5	274.6	211.2
Failure Stress (kPa)	190.5	273.6	211.0
Ultimate Strain (mm/mm)	0.143	0.155	0.133
Failure Strain (mm/mm)	0.170	0.161	0.135
Total Strain Energy Density (kJ/m^3)	25.1	29.4	19.2
Plastic Energy Density (kJ/m^3)	18.8	15.3	11.7
Total Strain Energy Density for 1.0 (kJ/m^3)	0.91	1.9	3.1
Total Strain Energy Density for 0.05 (kJ/m^3)	24.2	19.7	16.2

As was observed in the non-heated test results, the fracture strain, ultimate stresses, and total strain energy densities are greater in the specimens tested with an initial fast strain rate followed by a slow strain rate than specimens with the strain rates reversed.

Figure 32 shows a typical stress-strain curve for a specimen subjected to a varying strain rate with an initial strain rate of 0.05 s^{-1} and a second strain rate of 1.0 s^{-1}. Included in the figure are the results of the heated specimens when subjected to single strain rates of 1.0 s^{-1} and 0.05 s^{-1}.

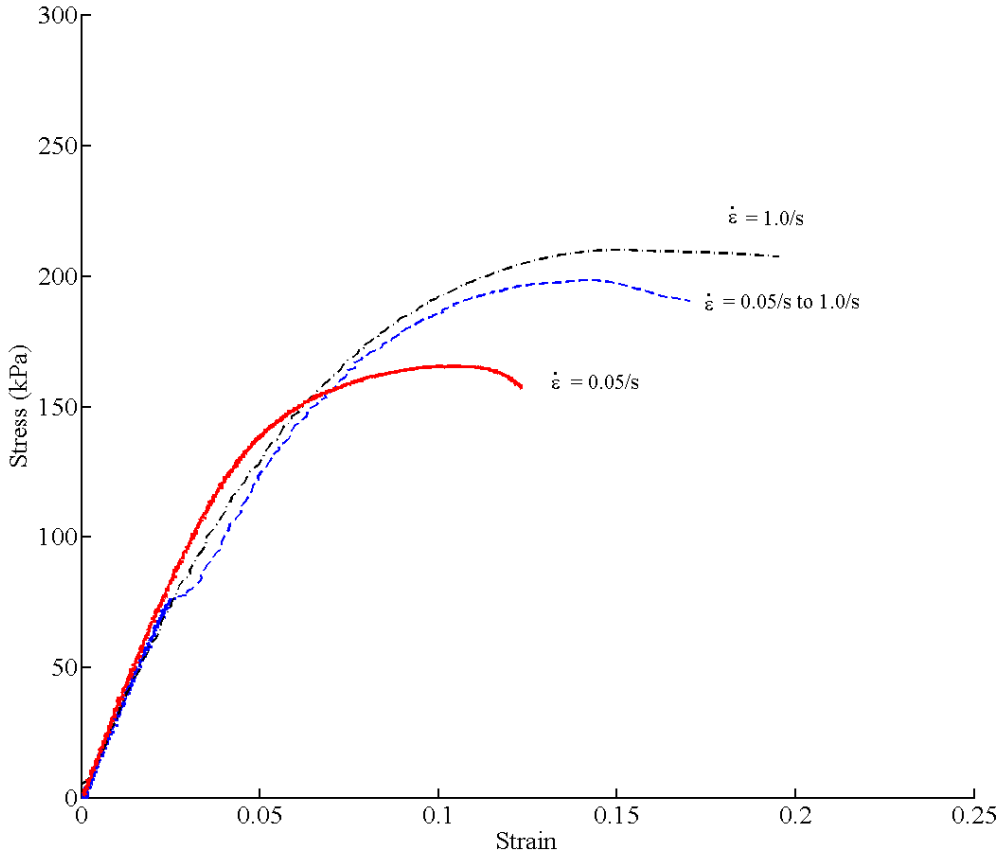

Figure 32. Varying strain rate results of heated specimens.

The testing of the heated specimens with varying strain rates yielded the same results as the non-heated specimens in terms of fracture strain and total shear energy density. The values of the failure strains and total shear energy densities of varying strain rates were between the initial and final strain rate values and they are plotted in Figures 33 and 34.

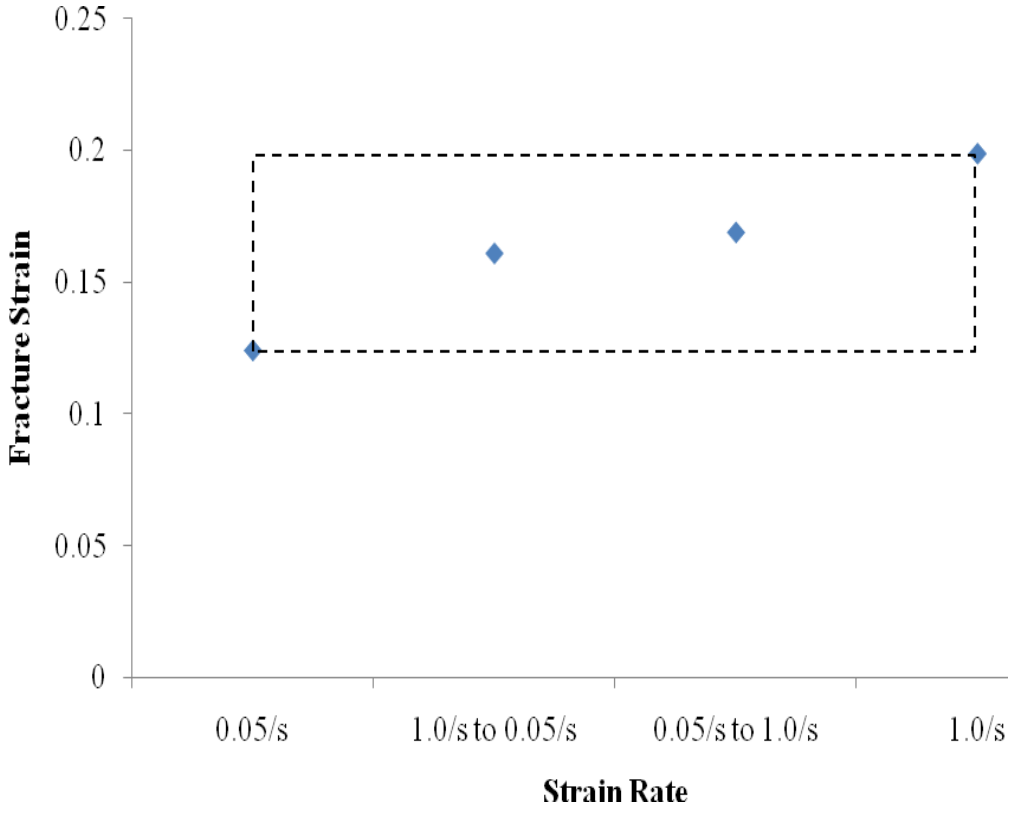

Figure 33. Fracture strain of single and multiple strain rates of heated specimens.

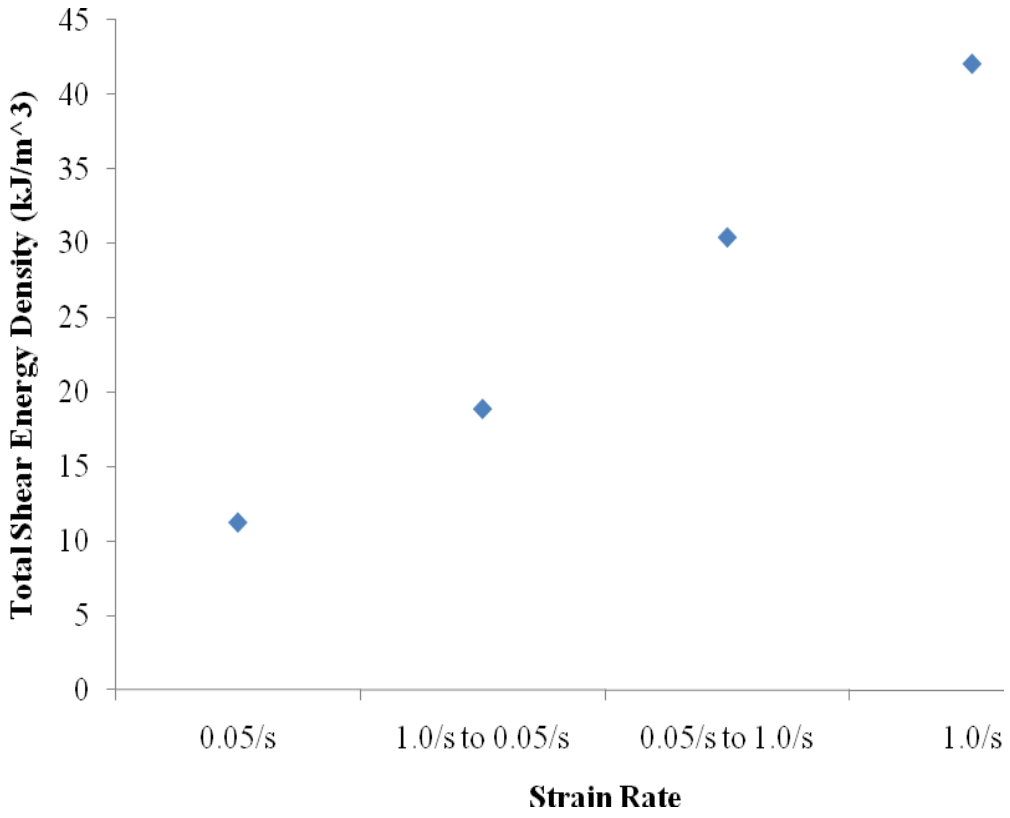

Figure 34. Total strain energy density of single and multiple strain rates of heated specimens.

Figure 35 shows the comparison of a heated and non-heated multiple-strain rate test. Similar to the single-strain rate comparison of heated and non-heated specimens, the ultimate strength of the non-heated is less than the heated specimen.

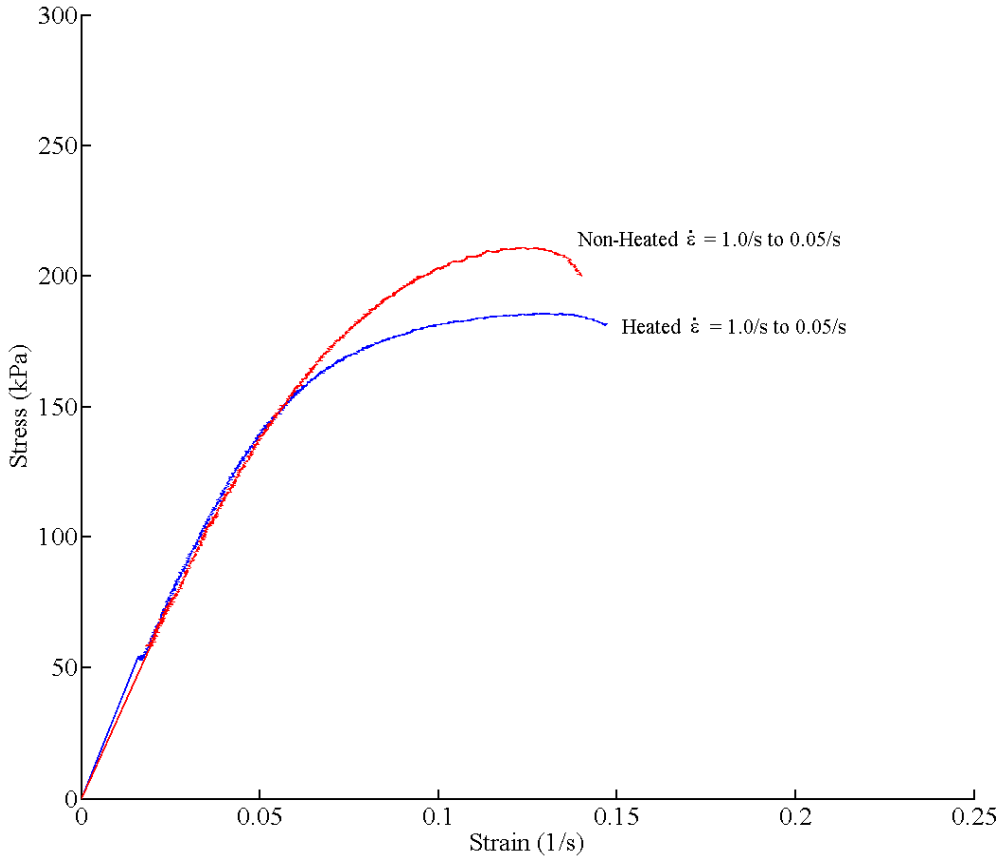

Figure 35. Comparison of a heated and non-heated multiple-strain rate test.

IV. FAILURE PREDICTION CRITERION

Analysis of the non-heated and heated multiple-strain rate tests revealed that all the fracture strains lie between the fracture strains of the two-single strain rates. Table 14 includes the results of the 24 multiple-rate strain tests from both specimens that were heated and not heated.

Table 14. Results of multiple-strain rate tests.

No.	1st Strain Rate (1/s)	2nd Strain Rate (1/s)	Transition Strain	Actual Fracture Strain
1	1.0	0.05	0.016	0.126
2	1.0	0.05	0.020	0.135
3	1.0	0.05	0.027	0.131
4*	1.0	0.05	0.047	0.106
5*	1.0	0.05	0.057	0.148
6*	1.0	0.05	0.072	0.148
7^	1.0	0.05	0.016	0.163
8^	1.0	0.05	0.020	0.166
9^	1.0	0.05	0.027	0.148
10*^	1.0	0.05	0.047	0.165
11*^	1.0	0.05	0.057	0.155
12*^	1.0	0.05	0.072	0.175
13	0.05	1.0	0.010	0.186
14	0.05	1.0	0.016	0.196
15	0.05	1.0	0.024	0.194
16*	0.05	1.0	0.031	0.157
17*	0.05	1.0	0.042	0.157
18*	0.05	1.0	0.057	0.154
19^	0.05	1.0	0.010	0.184
20^	0.05	1.0	0.016	0.163
21^	0.05	1.0	0.024	0.170
22*^	0.05	1.0	0.031	0.170
23*^	0.05	1.0	0.042	0.161
24*^	0.05	1.0	0.057	0.165

*: Transition strain was after yield stress. ^: Heated specimens

To predict the fracture strain, a ratio is used which consists of the average fracture strain of the multiple strain rates over the reference strain of the final single strain rate. To give an example of the reference strain, let's consider two specimens are fractured at the same strain rate but at different temperatures. The result will be two different fracture strains. The average of the fracture strains is the reference strain in Equation (5).

The 24 multiple-strain rate tests were divided into two groups. One group is the results from specimens tested at an initial strain rate of 1.0 s^{-1} transitioning to a final strain rate 0.05 s^{-1}. The strain rates were reversed for the second group. The fracture strains of each group are averaged and used in Equation (5) as strain average.

$$R = \frac{\varepsilon_{avg}}{\varepsilon_{ref}} \tag{5}$$

The result of Equation (5) of the first group is 1.33 and the result of the second group is 0.810.

Equation (6) is used to predict the fracture strain for specimens subjected to multiple-strain rates. As an example, for specimens subjected to an initial strain rate of 1.0 s^{-1} followed by 0.05 s^{-1}, the ratio from the first group, R, is multiplied by the reference fracture strain. The reference fracture strain is the fracture strain of the single-strain rate to which the specimen is subjected to last. In this case, the reference strain rate is 0.05 s^{-1} and the associated fracture strain for that strain rate must be used, taking into account whether the specimen had been heated.

$$\varepsilon_{fracture} = R * \varepsilon_{ref} \tag{6}$$

The predicted fracture strains are compared to the experimental fracture strains in Table 15 for non-heated specimens and Table 16 for heated specimens. The non-heated and heated specimens were listed in separate tables since the reference fracture strain of Equation (6) is different for non-heated and heated specimens even though the ratio, R, is the same for all specimens.

Table 15. Comparison of actual and predicted fracture strains of non-heated specimens.

1st Strain Rate (1/s)	2nd Strain Rate (1/s)	Transition Strain	Actual Fracture Strain	Predicted Fracture Strain	Error (%)
1.0	0.05	0.016	0.126	0.128	1.59
1.0	0.05	0.020	0.135	0.128	-5.19
1.0	0.05	0.027	0.131	0.128	-2.29
1.0	0.05	0.047	0.106	0.128	20.75
1.0	0.05	0.057	0.148	0.128	-13.51
1.0	0.05	0.072	0.148	0.128	-13.51
0.05	1.0	0.010	0.186	0.181	-2.69
0.05	1.0	0.016	0.196	0.181	-7.65
0.05	1.0	0.024	0.194	0.181	-6.70
0.05	1.0	0.031	0.157	0.181	15.29
0.05	1.0	0.042	0.157	0.181	15.29
0.05	1.0	0.057	0.154	0.181	17.53

Table 16. Comparison of actual and predicted fracture strains of heated specimens.

1st Strain Rate (1/s)	2nd Strain Rate (1/s)	Transition Strain	Actual Fracture Strain	Predicted Fracture Strain	Error (%)
1.0	0.05	0.016	0.163	0.165	1.23
1.0	0.05	0.020	0.166	0.165	-0.60
1.0	0.05	0.027	0.148	0.165	11.49
1.0	0.05	0.047	0.165	0.165	0.00
1.0	0.05	0.057	0.155	0.165	6.45
1.0	0.05	0.072	0.175	0.165	-5.71
0.05	1.0	0.010	0.184	0.161	-12.50
0.05	1.0	0.016	0.163	0.161	-1.23
0.05	1.0	0.024	0.170	0.161	-5.29
0.05	1.0	0.031	0.170	0.161	-5.29
0.05	1.0	0.042	0.161	0.161	0.00
0.05	1.0	0.057	0.165	0.161	-2.42

Figures 36 shows the prediction of the fracture strain for a multiple-strain rate specimen with an initial strain rate of 1.0 s^{-1} transitioning to a final strain rate of 0.05 s^{-1}. The transition strain is noted by point A, the actual fracture strain is at point B, and the predicted fracture strain is at point C. Figure 36 is the same as Figure 37, but the strain rates are reversed and the transition strain differs.

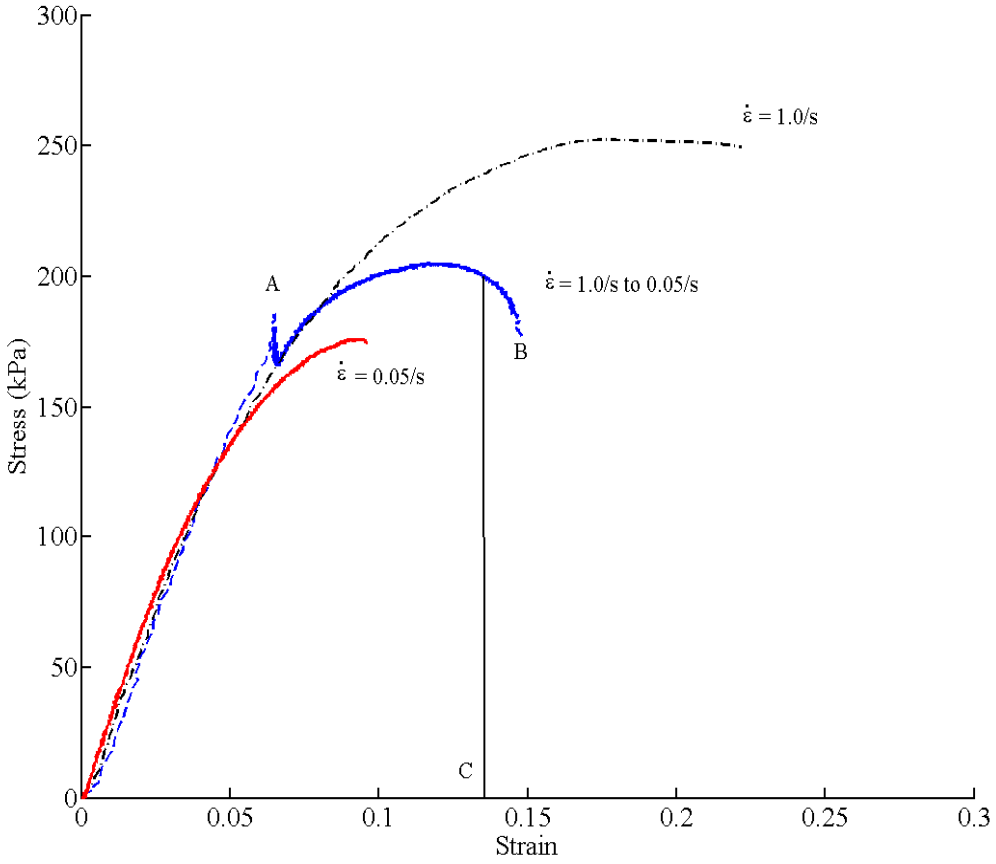

Figure 36. Predicted fracture strain compared to the actual fracture strain.

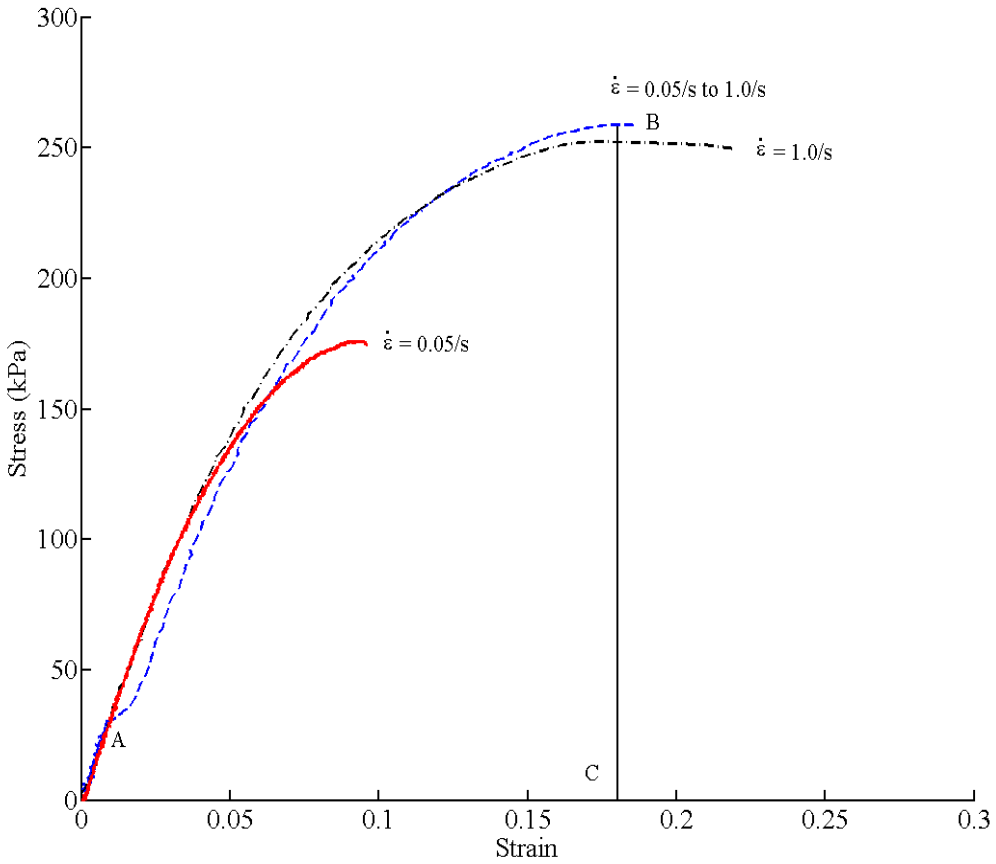

Figure 37. Predicted fracture strain compared to the actual fracture strain.

THIS PAGE INTENTIONALLY LEFT BLANK

V. CONCLUSIONS AND RECOMMENDATIONS

Uniaxial testing was conducted to investigate the mechanical behaviors of a solder joint under single and varying strain rate loading. In addition, the testing also included the heating of specimens to examine the mechanical behavior of the solder joint at an elevated temperature. In was noted that the elastic modulus of all the specimens tested decreased as the strain rate increased, while the yield and ultimate strengths increased noticeably. The heated specimens had much lower strengths than the unheated specimens. However, increase in ductility of the heated specimens resulted in higher fracture strains. It was also noted the fracture strains, ultimate strengths, total strain energy densities for specimens that were subjected to an initial fast strain rate followed by a slow strain rate had values higher than specimens tested with the strain rates reversed. Analysis of the fracture strain of the single and multiple strain rate tests revealed that the fracture strain from multiple-strain rate loadings fell between the fracture strains of the two single-strain rates. This allowed for the proposal of a simple failure criterion of predicting the fracture strain of a solder joint subjected to multiple strain rates by utilizing simple averaging techniques.

The current work may be extended in the following ways:

(i) Additional strain rates should be used between the range of strain rates that were selected in this thesis. This would give better resolution of the mechanical behavior of the solder joint and verify the trends observed in this study.

(ii) The copper-solder specimen should be subject to a wider range of temperatures as thermal stress is a major factor in solder joint failure.

(iii) Different compositions of lead-free solder should be used to see if the failure prediction method in this thesis is applicable to different solders.

(iv) More experiments should be conducted that examine the behavior of the solder joint under dynamic loading and unloading conditions of varying strain rates. These experiments should not only examine shock vibrations but also thermal stress and thermal cycling.

THIS PAGE INTENTIONALLY LEFT BLANK

LIST OF REFERENCES

[1] J. Gu et al., "Prognostics of electronics under vibration using acceleration sensors," in Proceeding for 62nd Meeting of the Society of Machinery Failure Prevention, Virginia Beach, VA, May 2008.

[2] R. Ross et al., "Solder Joint Creep and Stress Relaxation Dependence on Construction and Environmental-Stress Parameters," ASME *Journal of Electronic Packaging*, to be published.

[3] M. Celik and C. Genc, "Mechanical Fatigue of an Electronic Component under Random Vibration," *Fatigue & Fracture of Engineering Materials & Structures*, vol. 31, pp. 505–516.

[4] Y. Su et al., "Rate-Dependent Properties of Sn-Ag-Cu Based Lead Free Solder Joints," in *11th Electronics Packaging Technology Conference*, Singapore, 2009, pp. 283–291.

[5] H. Pang and X. Che, "Drop Impact Analysis of Sn-Ag-Cu Solder Joints Using Dynamic High Strain Rate Plastic Strain as the Impact Driving Force," in *Electronics Components and Technology Conference*, Singapore, 2006, pp. 49–54.

[6] M. Bayes, "Solder Joint Reliability," *Solder Joint Reliability* [Online]. Available: http://www.rohmhaas.com/electronicmaterials/interconnect_technical_site/attachments/Tech%20comm_%20Jul%2008%20English.pdf

[7] JEDEC Solid State Technology Association, 2003, "Board Level Drop Test Method of Components for Handheld Electronic Products," Arlington, VA, July, JESD22-B111.

[8] F. Qin et al., "Strain Rate Effects and Rate-Dependent Constitutive Models of Lead-Based and Lead-Free Solder," ASME *Journal of Applied Mechanics*, 2010, vol. 77.

[9] *Soldering Basics*, Circuit Technology Center, Inc., Haverhill, MA, 2009.

[10] M. Hoban and B. Lunt (1997 Spring). *Soldering* [Online]. Available: http://technologyinterface.nmsu.edu/spring97/spring97.html.

[11] P. Zarrow (2001, June). *The Real Cost of Lead-Free Soldering* [Online]. Available: http://www.itmconsulting.org/Column34-Real%20Cost%20of%20Lead-Free%20Soldering.pdf

[12] *ASM Handbook*, vol. 6, *Welding, Brazing, and Soldering*. Materials Park, OH: 1993, pp. 366–368.

[13] R. Kandpur, "Soldering, Assembly and Re-Working Techniques" in *Printed Circuit Boards: design, fabrication, assembly and testing*, New Delhi, India: Tata McGraw-Hill, 2008, ch. 13, sec. 2, p. 455.

[14] Z. Moser et al., "Wetting Action" in *Database of Lead-Free Soldering Materials*, Poland: Springer, 2007, ch. 2, pp. 9–11.

INITIAL DISTRIBUTION LIST

1. Defense Technical Information Center
   Ft. Belvoir, Virginia

2. Dudley Knox Library
   Naval Postgraduate School
   Monterey, California

3. Young W. Kwon
   Naval Postgraduate School
   Monterey, California

4. Jarema M. Didoszak
   Naval Postgraduate School
   Monterey, California

5. Andrew M. Luteran
   Naval Postgraduate School
   Monterey, California